In-Situ Continuous Monitoring of Catastrophic Phase Inversion and Viscosity of Pickering Emulsions

by

Upinder Bains

A thesis
presented to the University of Waterloo
in fulfillment of the
thesis requirement for the degree of
Master of Applied Science
in
Chemical Engineering

Waterloo, Ontario, Canada, 2018

AUTHOR'S DECLARATION

I hereby declare that I am the sole author of this thesis. This is a true copy of the thesis, including any required final revisions, as accepted by my examiners.

I understand that my thesis may be made electronically available to the public.

Abstract

Emulsions are used in the various field such as petroleum, pharmaceuticals, foods, cosmetics, paints, etc. Emulsions stabilized with solid nanoparticles are called Pickering emulsions. More recently, a growing awareness of using environment friendly products has led to more and more researchers to develop and modify natural materials. Starch nanoparticle might be a suitable candidate because they are environmentally friendly, safe and non-toxic. Also, from a practical point of view, starch nanoparticles are low cost, and rheological properties of their emulsions can easily be altered with the help of additives. Because of the unstable nature of these emulsions, continuous agitation is needed to keep the emulsion from separating. This makes the viscosity measurements a challenge, however this task was made possible at low shear rates under some controlled parameters.

In this study, an in-situ viscosity measurement method is used to investigate the viscous behaviour of O/W and W/O emulsions at a different volume fraction of the dispersed phase. For this purpose, rotational viscometer installed in a tank was used along with a high shear mixer. In this work, two sets of emulsions were formulated with starch nanoparticles to study their rheological behaviour. Also, Surfactant-stabilized O/W type emulsions were formulated with commercially known Triton X-100 non-ionic surfactant and compared with solid nanoparticles emulsions for rheology and stability. The emulsions viscosities and shear rate were measured at different concentrations of the dispersed phase and spindle rotation speeds.

Experimental results showed that, at low concentration of dispersed phase, emulsions exhibited Newtonian behaviour and at high concentrations of the dispersed phase, emulsions displayed non-Newtonian shear-thinning behaviour in that viscosity was dependent on the shear rate. This nature of the emulsions was confirmed as the viscosity measurements changed with spindle rotation speeds. Starch nanoparticles increased the viscosity of the emulsions and played a critical role in stabilizing emulsions by adsorbing at the oil-water interface. For water-in-oil emulsions, Pickering emulsions displayed phase inversion which was related to particle concentration.

Acknowledgements

I would like to express my sincerest gratitude to my supervisor, Dr. Rajinder Pal for his constant guidance, patience, support and encouragement throughout the course of this research. I deeply appreciate the opportunity to study and work under his supervision.

I would also like to express my gratitude to my labmates Sileola Ogunlaja, Arshdeep Singh and Sima Lashkari for their help and useful discussion. My gratitude is also given to graduated student Yifan Wu who helped during the initial stage of the project.

I would like to thank all friends and colleagues who have helped and supported me. Finally, a very special thanks to my parents and brother for their encouragement, support and understanding.

Table of Contents

List of Figures

List of Tables

Chapter 1
Introduction

1.1 Fundamentals of Emulsions

Emulsion is formed when two immiscible liquids are mixed together in a container and then shaken, one of the two phases become a collection of droplets that are dispersed in the other phase. They are dispersions in which a liquid is dispersed in a continuous liquid phase of the different composition. In this two-phase system, one of the liquid is aqueous while the other is hydrocarbon and referred to as oil. Depending upon which kind of liquid forms the continuous phase, two types of the emulsion are readily distinguished as either oil-in-water (o/w) or water-in-oil (w/o) emulsions [1]. The phase that makes up the droplets in an emulsion is referred to as the internal or dispersed phase, whereas the substance that makes up the surrounding liquid is called the external or continuous phase [2].

1.2 Emulsion Stabilizers

Stabilizers are used to decrease the interfacial tension between the oil and water phases. The important function is to form a protective coating around the droplets, thereby preventing them from deformation [3]. In our work, we used two main stabilizers i.e. a non-ionic surfactant and starch nanoparticles for emulsions.

1.2.1 Surfactants

Surfactants are organic compounds that exhibit a double affinity, i.e. they have at least one polar group and one apolar group. Because of its duality, surfactants molecules have a great tendency to migrate and modify the surface properties of the liquid. Surfactant molecules adsorb at an interface and help in lowering interfacial tension by providing an opposite expanding force. Surfactants are classified based on their solubility in water and/or oil, also known as HLB number. The HLB number (hydrophilic-lipophilic balance) is a numerical

system which used to classify surfactants. It is a ratio of a number of hydrophilic groups to lipophilic groups in surfactant molecular structure. A molecule with high HLB number can be used to stabilize oil-in-water emulsions because it has a higher ratio of hydrophilic groups and would easily dissolve in the aqueous phase.

In the past two decades, there has been considerable interest in a new class of materials called polymeric surfactants derived through polymerization of surface active monomers. Consequently, there has been a focus on replacing synthetic surfactants with other alternatives that natural and labeled friendly. For example, a detailed study on emulsion stabilizing properties between a natural surfactant (Q-Naturale) and a synthetic non-ionic surfactant (Tween-80) was done by Y. Yang et al. [4]. The study showed that Q-Naturale exhibited similar interfacial properties as Tween 80 and produced oil-in-water emulsions with relatively smaller droplet sizes than Tween 80.

1.2.2 Solid Nanoparticles

Nanoparticle can be used as a replacement to classical surfactants for the stabilization of emulsions. Pickering emulsion has many benefits with respect to classical emulsions in most applications of emulsions. Surface modification of solid nanoparticles gives control to wetting behaviour which offers the possibility of a wide range of emulsions including very stable double and course emulsions [5]. During the past few years, nanoparticles and microparticles have been of great interest for their effective role in the stabilization of liquid droplets. Solid-nanoparticle emulsions, also commonly known as Pickering emulsion, stabilize emulsion droplets against coalescence by forming a steric barrier at the oil-water interface. Figure 1.1 shows a schematic diagram of an oil-in-water emulsion stabilized by a surfactant and solid nanoparticles**.**

Many studies related to the rheology of nanoparticles stabilized emulsions have been reported. For example, S. Ge et al. [6] worked with four different types of starch nanoparticles is the sizes ranging from 50-700 nm for their influence on the stability of Pickering emulsions. They reported that stability of emulsions was influenced by the contact angles of starch nanoparticles. Contact angle is dominated by particle size, SNPs with size ranging from 100

to 220 nm were found best suitable for preparing Pickering emulsion. Dargahi-Zaboli et al. [7] (2017) studied the rheological properties of hydrophobic silica nanoparticles forming stable water-in-oil invert emulsion which had the desired properties of meeting drilling fluid requirements. The influence of particle concentration and drop size distribution was analyzed by Hohl et al. [8], who concluded that drop size distribution increased with the hydrophobicity of silica particles. Higher particle concentration in the oil phase resulted in smaller Sauter mean diameters and higher viscosity. Schematic representation of oil-in-water emulsion stabilized using a surfactant and solid particles.

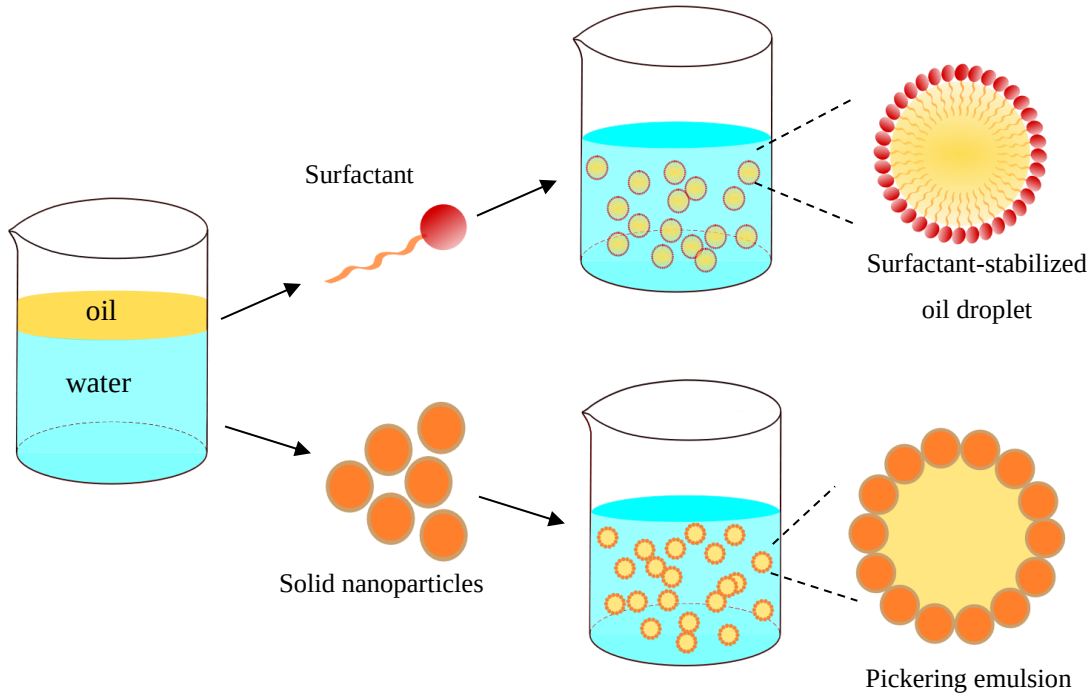

Figure 1.1 Schematic representation of oil-in-water emulsion stabilized using a surfactant and solid particles

1.3 Phase Inversion

Phase inversion is a phenomenon that takes place when the structure of the emulsions inverts due to dilution with additional internal phase. It can be achieved by changing any one of the variables such as oil/water ratio, pressure, temperature, salinity and cosurfactant [9]. Generally, there are two main ways to induce phase inversion that has been reflected in the literature. First one is catastrophic phase inversion in which disperse phase reverts to the continuous phase when its volume is gradually increased. In this type, highly concentrated emulsions are formed, and further increasing amounts of the dispersed phase is added to the system with continuous mixing as shown in figure 1.2. A point is reached where droplets are tightly packed together, and the system can no further intake more water content. At this critical point phase inversion occurs where emulsions change from W/O to O/W. Second one is phase inversion temperature (PIT) which occurs due to change in temperature without change in the system composition.

Electrical conductivity measurement is mostly used to determine phase inversion since the conductivity of O/W, and W/O is different by several orders of magnitude. In a very small range of time conductivity reading shows a steep variation at the inversion point. The time to reach the phase inversion (delay time) could vary from instant inversion to absolutely no inversion at all [10]. Ogunlaja et al. [11] investigated the effect of starch nanoparticles on catastrophic phase inversion. They reported a delay in phase inversion on increasing the NPs concentration in the aqueous phase.

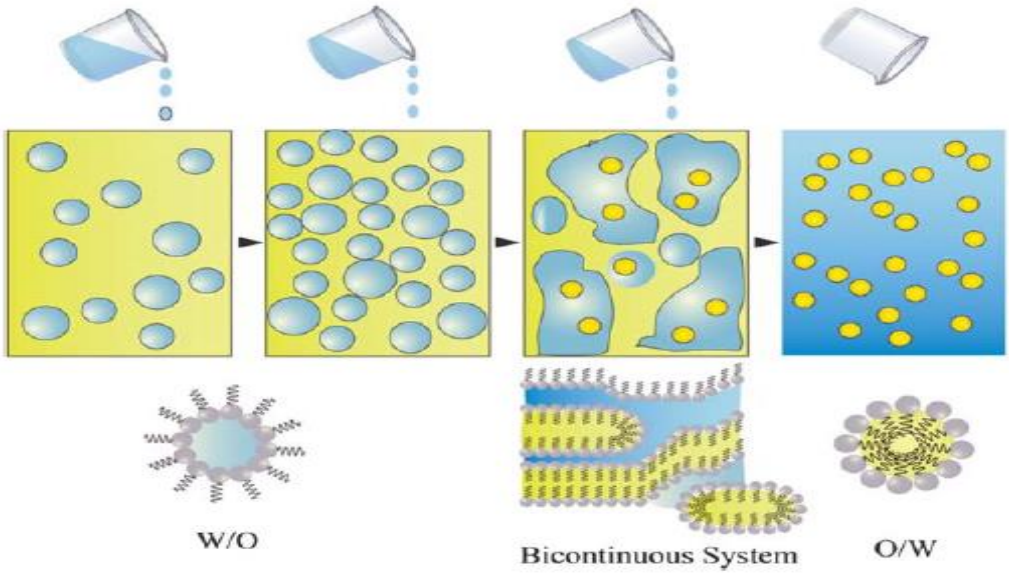

Figure 1.2 Schematic representation of Catastrophic Phase Inversion [14]

1.4 Emulsion Stability

Emulsion is formed by agitating two phases of different density, e.g., pure oil (lower density) and pure water (pure water). The two phases rapidly revert to its individual components due to low activation energy between the two states. This phase separation occurs due to a collision between droplets which tend to merge with their neighbors [2]. The thermodynamic instability of (macro)emulsions can be illustrated in terms of free energy change between initial and final state (Hunter, 1989) [12].

$$\Delta \boldsymbol{G_{formation}} = \boldsymbol{\gamma \Delta A} - \boldsymbol{T \Delta S_{config}} \qquad \textbf{1.1}$$

After emulsification, there is an increase in interfacial area, so change in interfacial free energy ($\gamma \Delta A$) is always positive. On the other hand, in the emulsified state the number of arrangement of droplets is much greater which is why ($-T\Delta S_{\mathrm{config}}$) is always negative. But in most emulsions, the entropy term is negligible and is ignored. Thus, the formation of an emulsion is always thermodynamically unfavorable. Still, emulsions can attain kinetic stability with different droplet sizes at same composition. Kinetically stable emulsion contains smaller

droplet than thermodynamically unstable emulsion and has a longer shelf life (because of difference in interfacial area, ΔA) [2].

Instability in emulsions is explained through a variety of physicochemical mechanisms shown in figure 1.3. Most common form of instability in emulsions is gravitational separation which can be in the form of sedimentation or creaming. Sedimentation is settling of droplets at the bottom due to a higher density than the surrounding liquid, and conversely, if they have lower density, they tend to move upward, which is referred to as Creaming. At high droplet concentration, the system is close-packed which slows the rate of separation [13].

Due to constant motion (because of gravity, thermal energy or mechanical forces), droplets frequently collide and sometimes they form aggregate. Depending upon the interactions between the droplets (attractive or repulsive), they may remain aggregated or move away from each other. Flocculation depends upon a number of droplets encounters and increases if collision frequency is increased by any factor [13].

Droplets are separated by a thin film that keeps them separated and with rupturing of this thin film oil and water phase can attain a thermodynamically stable state. Coalescence is a process where two or more droplets after collision merge together to form a single large droplet. When the size of droplets is increased, they tend to migrate fast and sediment or cream more rapidly [13].

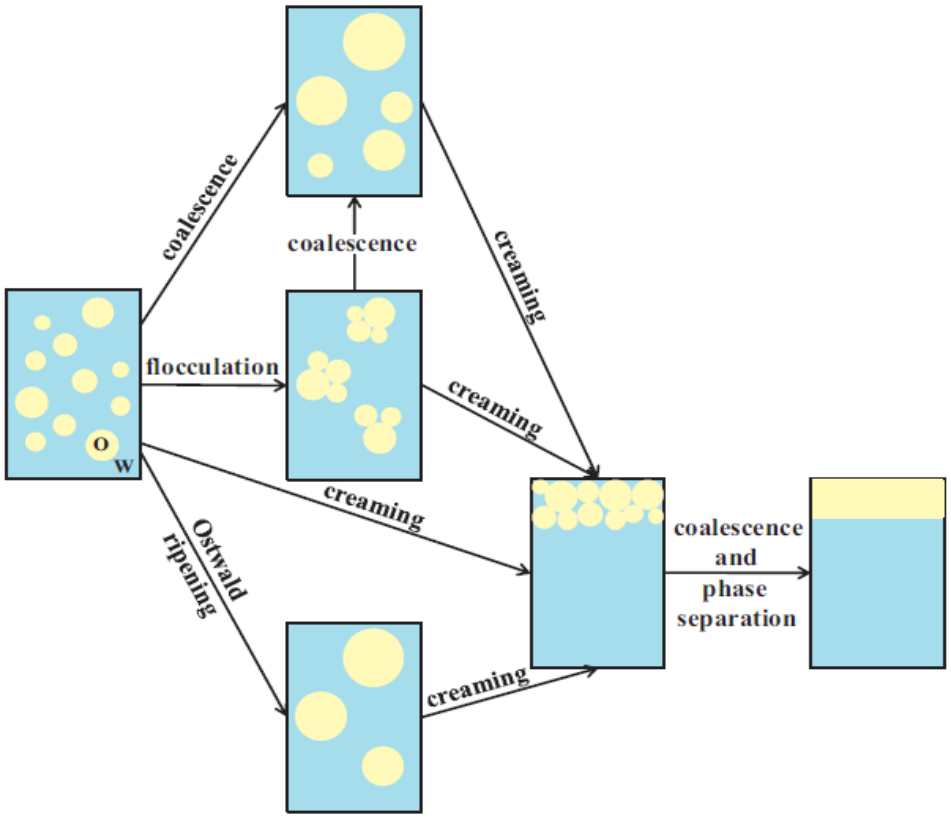

Figure 1.3 Schematic diagram of common destabilization mechanisms: coalescence, Ostwald ripening, flocculation, creaming and sedimentation [36]

1.5 Importance of the Research

In recent years, there has been a rapid growth of interest in eco-friendly materials that are less toxic to humans and the environment. The production growth in the current market is focused on compliance to profitability and environment sensitivity. Emulsions are used in many major industries such as: food, pharmaceutical, petroleum, and cosmetics. Nowadays, Pickering emulsions are substituted for traditional emulsions for most applications because they retain the basic properties of surfactants without causing any adverse side effects. For instance, crude oil emulsions are formed at several stages during heavy oil production. Due to the high viscosity of emulsions, several challenges are encountered during production, transferring and metering of these emulsions. Particle-stabilized emulsions have a unique

feature of inverting the system to the water phase and solving these problems by reducing its viscosity.

To study and understand emulsion behaviour, rheological characterization is an important tool. For example, water is produced along with oil during crude oil production and as the concentration is varied, phase inversion might occur during the process. An abrupt change in viscosity can occur at this point resulting in large pressure drops. Also, multiple phases of oil, water and sand are frequently encountered and pose a serious challenge in measurement techniques. Laboratory testing is needed to answer several difficult questions such as what is the emulsion viscosity-temperature profile? What kind of fluid will be produced an oil-in-water or a water-in-oil emulsion and the size of the droplet? Thus, viscosity measurement of two-phase mixtures of oil and water is very crucial to the industry for evaluating the technology to operate under harsh conditions.

Currently, viscosity measurement available for multi-phase mixtures is a challenge and still must be done offline. Hence, the need for taking the sample from a flow which is not a homogenous does not represent a fair accurate measurement. Traditional laboratory viscometer has some limitations; one would take samples one by one out of the process and examine then. Viscosity can be directly affected by the temperature, flow, air and other variables that can be different from what they are in actual process.

While there are non-intrusive measurements available for measuring density, droplet size, and flow rate, viscosity measurement is not possible without an intrusive object. The reason behind this is that viscosity is measured when there is a resistance to the flow of fluid. Thus, measurement forms like microwave, ultrasound, use of laser and other gets ruled out.

1.6 Thesis Objectives

The broad objective of this work will be on the experimental study of viscosity behaviour of Pickering emulsions in an agitation vessel. Following are the specific objectives of this work:

1. To investigate in-situ viscosity measurement techniques using rotational viscometer. Implement the rotational viscosity measurement to measure the viscosity of two-phase liquid mixtures and gain insight into phase inversion phenomenon using this technique.
2. To study the behaviour of starch nanoparticles Pickering emulsions at different dispersed phase volume.
3. To identify the system that shows a high degree of phase inversion and to study its behaviour from a viscosity point of view. For example, a strong correlation is observed between nanoparticles concentration and viscosity behaviour.
4. To study the effect of nanoparticle on the catastrophic phase inversion and identify the concentration ranges of the phase inversion.
5. Finally, to study the separation of the dispersed phase and the stability of the emulsions with respect to coalescence.

Chapter 2

Review of In-line Techniques for Viscosity Measurement

In many industries such as chemistry, chemical, petroleum, food, cosmetics, etc., the most important rheological measurement and a parameter for product characterization is viscosity [14]. Rheological characteristics can be determined using off-line and on-line methods. In off-line testing, one would take samples out of the flowing material in a process, on the other hand, on-line techniques provide continuous monitoring which is important in process control and design [15]. In most cases, emulsions exhibit a complicated behavior which demands for accuracy in viscosity measurement. There are various types of viscometers that are available for measurements of viscosity. Most viscometers used in the laboratory are labor intensive and can measure viscosity at the single shear rate at a time. Hence, for multiple viscosity measurements at different shear rates, one must repeat the process [16].

Viscometers used in the lab are very accurate but are unsuitable for online measurement for many reasons such as poor portability, or sensitiveness to external vibrations [17]. Also, many different variables such as temperature, shear rate, the flow rate would be different laboratory testing. On-line viscosity measurement is a better way to reduce the time required in the analysis as compared to sampling which is slow, disruptive and often misleading.

2.1 Rotational Viscometers

In the early decades of the nineteen century, many versions of rotational viscometers were available in the market. Some of the earliest commercial viscometers were manufactured by Eimer and Amend of New York, the Searle instruments by Pye Company of Cambridge and Brookfield company. Many improvements to design and speed of the rotational viscometers have been made over the time, especially by Brookfield company. In a coaxial cylinder type rotational viscometer, a cylinder is set to rotate inside a hollow cylinder which contains test fluid. Viscosity is calculated from the torque experienced by the cylinder due to viscous drag forces. Both Newtonian and non-Newtonian fluids can be tested at different shear rates under steady-state conditions. Rotational viscometers have three main categories based

on their design: 1. Co-axial cylinder viscometer; 2. Cone and plate viscometer; 3. Parallel plate viscometer.

Figure 2.1 [18] presents a basic design of *coaxial-cylinder viscometer*. The basic structure of viscometer consists of an inner stationary cylinder of radius R_1 and outer rotating cylinder of radius R_2. The test fluid is made to rotate in the outer cylinder at a constant speed or shear rate. However, sometimes inner cylinder is rotated, and the outer cylinder is kept stationary for measuring higher viscosity. The dynamic viscosity of the fluid is measured by resultant torque shown by angular deflection of the spring.

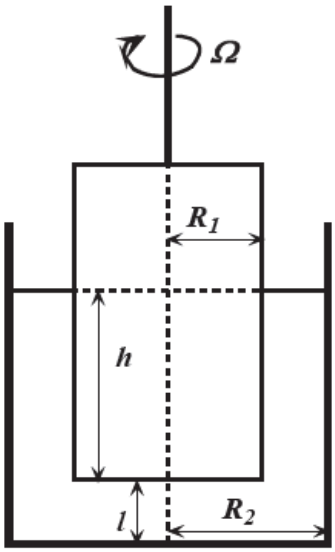

Figure 2.1 Basic Design of coaxial-cylinder viscometer [18]

Most of the existing commercial available laboratory rotational viscometer are manufactured to work offline. Although much information can be gathered using these viscometers but for on-line operation and acquiring a detailed knowledge of non-Newtonian fluids an automated on-line viscometer is needed. Some researchers have tried using rotational viscometers for performing on-line viscometry by designing modifications. Cheng and Davis [19] suggested three main requirements for a rotational viscometer to perform on-line viscometry operation. These requirements needed rotational viscometer to operate at a range of rotational speeds, to have speed change automation and an output signal for torque

measurement. In their work, they took a conventional manual viscometer and modified its arrangement meeting above listed requirements.

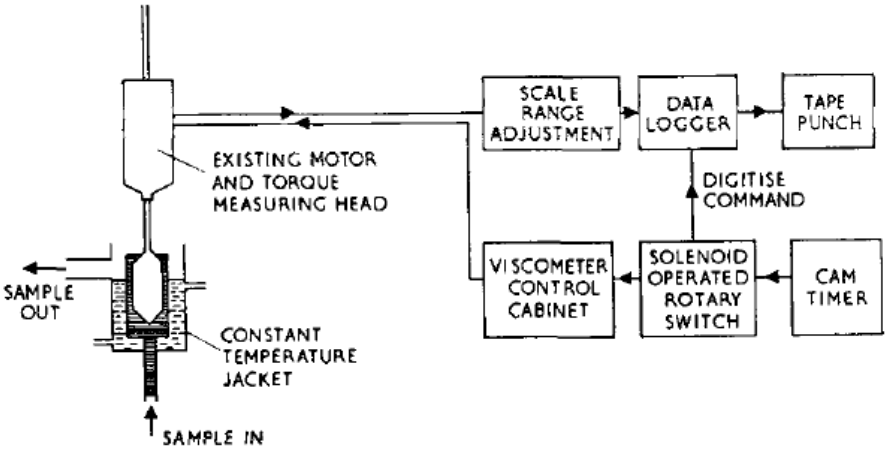

Figure 2.2 A modified arrangement of rotational viscometer used by Cheng and Davis[19]

The two-main modification in the above arrangement was replacing the manual speed controller with an electric rotary solenoid controlled by cam timer and using a special vessel for fluid inlet and outlet making viscometer capable for on-line operation (figure 2.2). They did encounter a problem in this geometry when measurements were made in a continuous flow. The bob immersed inside the vessel became too unstable, however the authors suggested to operate viscometer without a continuous flow and injecting fluid sample at each speed cycle.

Kawatra & Bakshi [20] used a similar approach to measure to the on-line viscosity of slurries using a Brookfield rotational viscometer. The system was designed to handle the problem of solids settling in slurries. They mixed slurry in an overhead tank, and passed it through the space between spindle and tube to prevent solids from settling (figure 2.3). Although, they did too interrupt the flow to take measurements as to prevent any additional forces to act on spindle due to slurry stream.

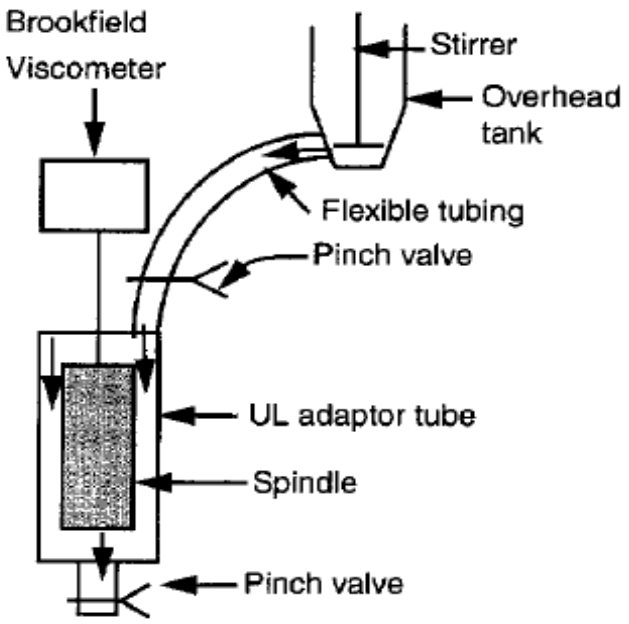

Figure 2.3 Rotational viscometer set-up [23]

Cone and plate viscometer are very commercially popular used rotational viscometers. It consists of cone shape geometry of large apical angle and flat plate normal to its axis as shown in figure 2.4 [18]. The first design of cone and plate viscometer was given Mooney and Ewart.

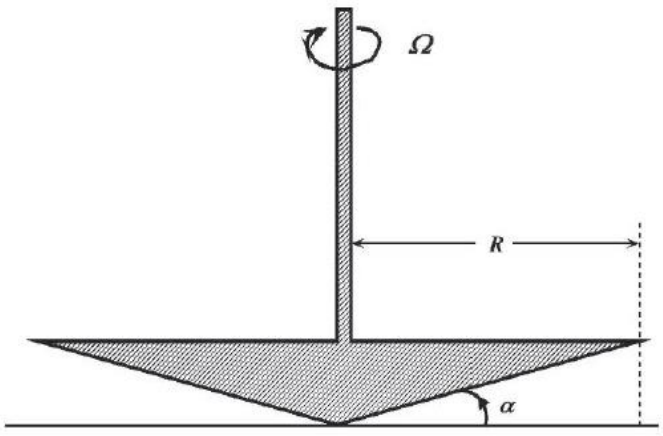

Figure 2.4 Cone and plate viscometer [18]

Several researchers have used *rotating disk viscometer* for calculating shear stress and viscosity. The original design of parallel or rotating disk geometry was suggested by Mooney. It consists of two dies forming a cylindrical cavity inside which a disk is rotated as shown in figure 2.5 [21]. Although, many researchers have concluded that it may not be the best instrument for viscosity measurement due to an issue like wall slip [22], instability of fluid and high Reynolds number.

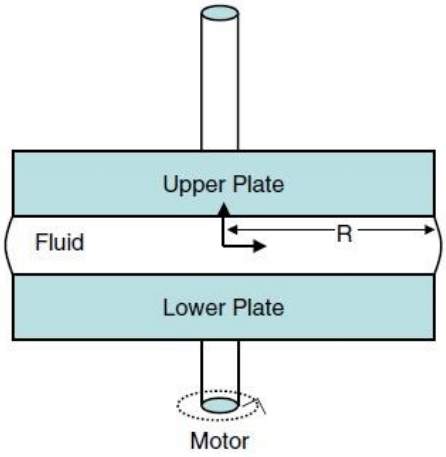

Figure 2.5 Conventional parallel-plate viscometer arrangement [21]

A new process viscometer that uses rotation as well as pressure build up by the fluid to measure viscosity was presented. *Dynamic inline viscometer* takes advantage of rotation method and provides freedom to be installed in the tank, in-line or in a bypass. It works on the same principle based on a hydrodynamic effect by which shear stress in the fluid is induced by the relative motion between the two surfaces. This stress leads to the formation of a lubricating film separating the sliding surfaces. If the film is wedge-shaped, the pressure to carry the load is developed, and this distribution of the pressure depends on the viscosity and surface velocity of the fluid [23]. The working principle is shown in figure 2.4 [24].

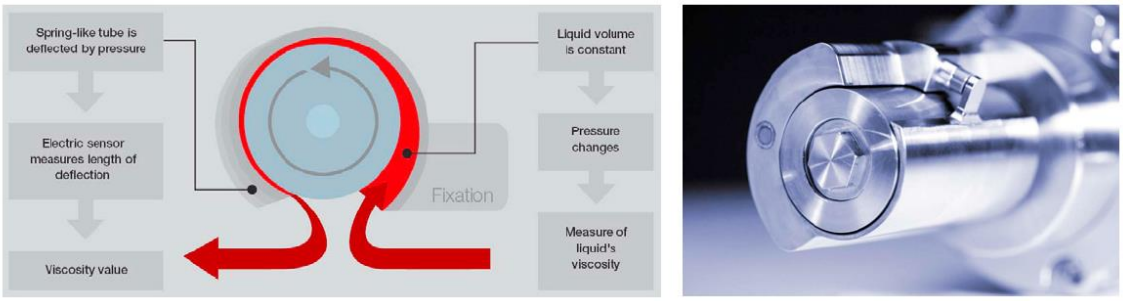

Figure 2.6 Functional principle and photograph of fluid dynamic inline viscometer [24]

Inline viscometer consists of a rotating cylinder and a stationary outer surface which creates a wedge-shaped gap. The action of rotor causes fluid to enter through a fixed surface entry and exit through sliding outlet. Pressure rise between the gap induces a slight displacement of the outer surface which is directly proportional to fluid viscosity. Inline viscometer can easily measure viscosity ranging from 1 to 2000 mPas. The author used inline viscometer with Newtonian and non-Newtonian fluid at three different shear rates of 88, 220, 352 s^{-1}. The instrument was found to be insensitive to external vibration or pressure jumps [24].

2.2 Tube Viscometry

Tube rheometry offers simple and quick on-site measurements of fluids over a wide range of shear rates. The first viscometer was that of Poiseuille in 1840, and even after more than 170 years, the fundamental design of these viscometers has not changed much. Goveir and Aziz defined tube viscometer as "a device that causes a sample of fluid to flow at a measured rate in laminar motion under a measured pressure gradient through a precision bore capillary tube of known diameter and length." Shear stress and shear rate can easily be calculated by measuring the pressure drop and flow rate across the tube [25]. Hagen-Poiseuille equation for a Newtonian fluid in laminar flow gives:

$$\eta = \frac{\pi D^4 (\Delta P/L)}{128Q} \qquad \textbf{2.1}$$

Where Q is the flow rate, ΔP is the pressure drop across a tube of know length L, and D is the internal diameter.

Capillary tube viscometer operates at relatively high shear rates under normal operating conditions. Cho et al. introduced a new device called scanning capillary tube viscometer for continuous viscosity measurements over a range of shear rates. It consisted of a charged coupled device (CCD), a rising tube, a capillary tube and a reservoir. The charge-coupled device was used to measure the variation in level of fluid in rising tube (figure 2.6 (a)). The viscometer was capable of producing viscosity data at a very low shear range up to 5 s^{-1} [16].

The concept was further developed by introducing a second capillary tube for increasing accuracy of viscosity measurements at very low shear rates (figure 2.6(b)). Authors reported satisfactorily measurement using dual-capillary tube viscometer at shear rate as low as 0.1 s^{-1} [26].

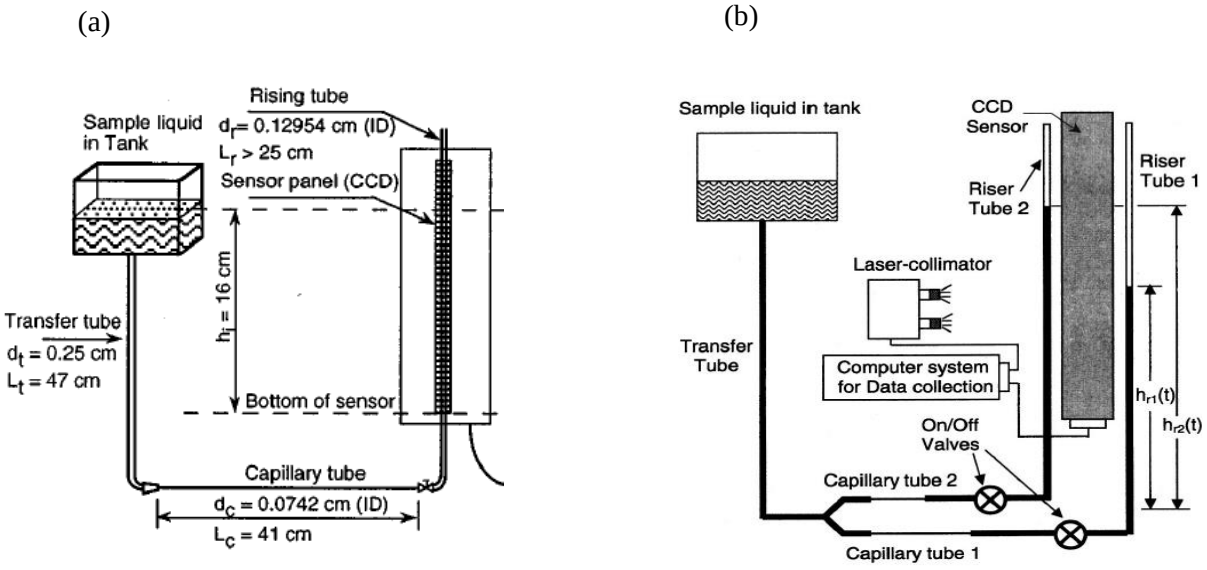

Figure 2.7 Sketch of scanning single(a) and double(b) capillary tube viscometer [20] [28]

Kawatra et al. [29] developed and presented an on-line pressure rheometer for viscosity measurements suitable especially for slurries. The authors have developed this rheometer using a sealed vessel with a steel tube of adjustable diameter and pressure transducers across the tube. One end of the rheometer is connected to a fluid line and the other end to the sealed chamber (figure 2.7). Data was collected from pressure transducer which measures pressure across the stainless-steel tube of adjustable diameter. They reported on-line viscosity measurement of slurries at a shear rate ranging from 0 to 10^4 1/sec. The equation they used to calculate shear rate and shear stress are as follows: [27]

$$\gamma = (8Q/DA) \quad \textbf{2.2}$$

$$\tau = \Delta P * D/4L \quad \textbf{2.3}$$

where is ΔP is pressure difference across tube; D is tube diameter; L is the length of the tube; Q is the flow rate, and A is the cross-sectional area of the tube.

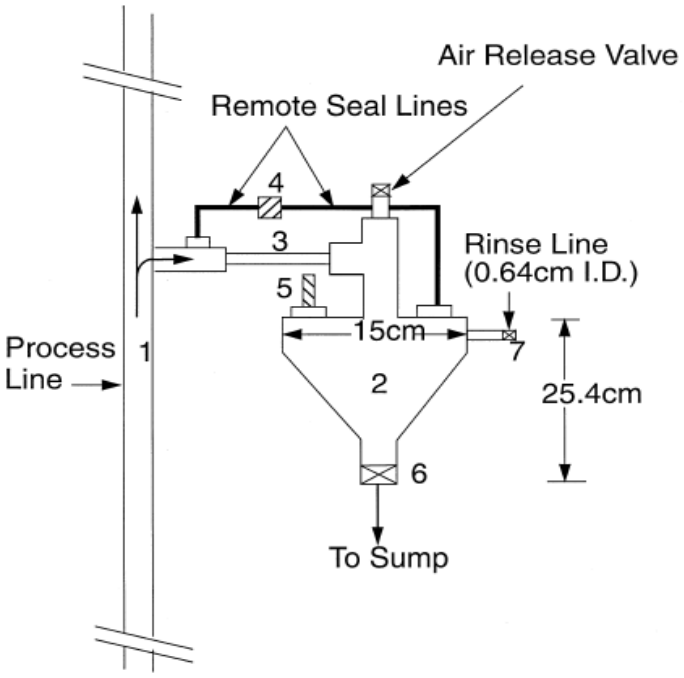

Figure 2.8 Line diagram of viscometer used by Kawatra et al**.** Legend: Legend: 1. process line, 2. vessel, 3. stainless steel tube, 4. differential pressure transducer, 5. absolute pressure transducer, 6. Drain valve, 7. water valve [29]

Coriolis mass flow meter are devices that are used to measure mass flow, fluid density, and temperature. Paul Kalotay discussed the use of assembling an on-line viscometer using a Coriolis mass flow meter and a differential pressure transmitter. The mass flow meter consists of flow tubes of constant diameter, and by implying Hagen-Poiseuille formula of pressure drop across these tubes viscosity was measured. However, the author pointed several factors that limit the use of this viscometer. Flow meter was only applicable to measurements of Newtonian fluids. Also, the Hagen-Poiseuille formula is valid for laminar flow.

2.3 Vibrational Viscometers

Conventional vibrating type viscometer exploits the frequency resonance curve obtained under external excitation for measurement of viscosity. Depending upon the amount of viscous force acting on oscillator submerged in liquid, vibrational viscometers generate peaks in frequency response curves. The simplest way to understand the concept behind vibrational viscometers is by analyzing a damped spring in a liquid. The viscous forces of liquid affect these damped vibrations of the spring, and an external restoration force is used to maintain constant oscillations [28]. The amplitude of these vibrations is very small usually, about μm in range. Viscosity of the fluid can be related to the power required to maintain these oscillation by the equation 2.1, where η_e is emulsion viscosity and ρ_e is its density.

$$\text{Power} = a(\sqrt{\rho_e}\eta_e) \qquad \textbf{2.4}$$

G. Wang et al. [17] designed and fabricated a self-sensing contact resonance viscometer using a sensing slice attached perpendicularly to a piezo-electric cantilever through a layer of stainless steel sheet as shown in figure 2.9. During measurement, the sensing in-plane immersed in the fluid oscillates due to vibrations by the piezoelectric cantilever. Based on the measurement of resonance frequency and quality factor (Q value), the electromechanical impedance of the cantilever is derived and used to calculate dynamic viscosity and density. They conducted online viscosity measurement with glycerol-water solutions, and the results coincided and agree well with those measured using a standard rotatory viscometer.

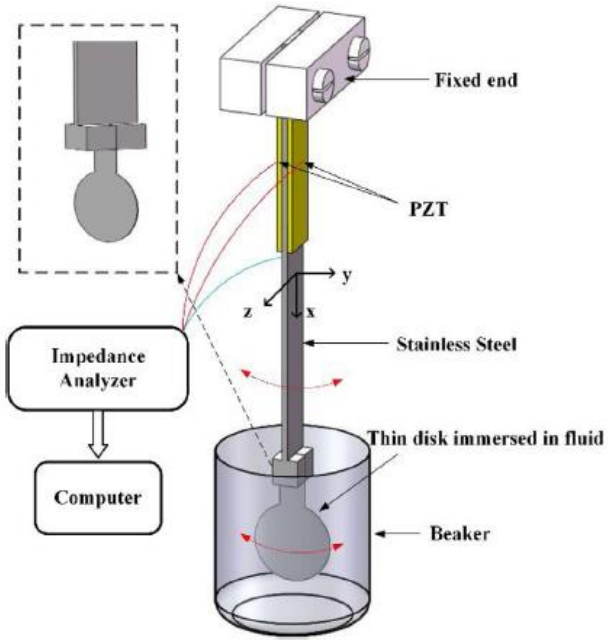

Figure 2.9 Shows the setup for viscosity measurement using Piezoelectric Cantilever [21]

A similar design (fig. 2.10) was proposed by Higashino et al. [29], but they used a cantilever driven by a piezo-actuator to generate self-excited oscillations using positive velocity feedback instead of producing frequency response curves and high Q factor values of external excitations. This method allows the measurement of high viscosity fluids by using a feedback force which compensates for the energy dissipation and oscillates disk generating self-excitations. A laser displacement sensor was used to measure the displacement x of the cantilever from its fixed end. The signal from the displacement sensor is used to determine critical variable gain required to generate self-excited oscillations. They proposed good results of viscosity measurements with errors less than 4%.

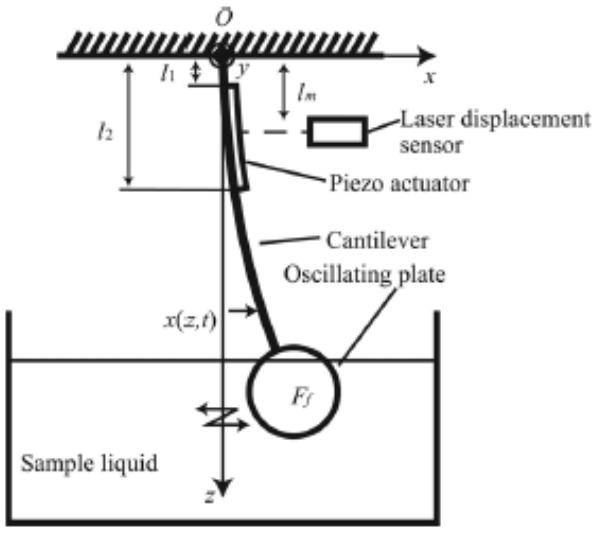

Figure 2.10 Model representing self-excited vibrational cantilever viscometer [30]

V. Chang et al. (1995) [31] used a mechanical device as a sensor for making on-line viscosity measurement of non-Newtonian fluids. They used software based on a learning algorithm called neural network. This neural network used mathematical models to convert input voltages signal to output viscosity and shear rate. Viscosity sensor received an input voltage (a.c.) and triggered oscillation in metallic blade due to vibration in the magnet. This oscillation of the blade results in energy dissipation in the fluid and induces a signal in the output coil. This output voltage was then used to estimate viscosity and shear rate. The layout of the sensor used is shown in figure 2.10. Although, the viscosity sensor was able to generate rheograms of non-Newtonian fluids. But direct estimation of viscosity and shear rate from voltage values was not reported, instead authors used viscosity and shear rate parameters (P_v and P_s) to associate real viscosity and shear rate. For this, they used to a calibration curve obtained using laboratory viscometer to relate these parameters with real viscosity and shear rate. The viscosity and shear rate parameters were defined as: $P_v = R^2/V_o$; $P_s = V_i^2/R^2$; where $R = (V_i/V_o)^2$, V_i is input voltage, and V_o is output voltage.

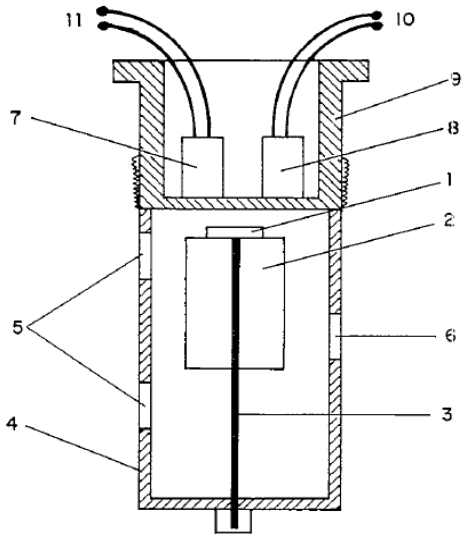

Figure 2.11 Schematic of viscosity sensor: 1. Magnet; 2. Steel blade; 3. Elastic rod; 4. Base cylinder; 5. Fluid entry; 6. Fluid exit; 7. Output coil; 8. Input coil; mounting body; 10 input cables; 11 output cables [31]

2.4 Mixer-type Viscometers

The challenging task when using conventional rheometers is a rheological characterization of complex fluids. Some fluids go through phase separation or partial destruction of their basic constituents when subjected to sampling rheology measurements. An alternative solution to such problem is to use mixer-type viscometry in which a mixing device is rotated in a fluid inside a cylindrical tank. Mixing devices are used to provide continuous mixing and at the same time rheological characterization of fluid. Conventional rheometers use defined geometries and controlled flow kinetics to get viscosity/shear rates curves. However, in case of mixing devices, a more detailed analysis is needed to get shear rate-shear stress relationship that includes monitoring of torque, the speed of rotation and power consumption.

Many researchers have used Couette analogy in modeling and analysis of torque/speed data for different types of mixing devices. This approach is based on a method developed by Bousmina et al. (1999) to calculate shear rate and viscosity from torque and rotor speed. In

their approach, they used two equivalent virtual concentric cylindrical bobs to represent a dual mixing device which exerts the same torque while rotating in a cylindrical chamber (figure 2.11). They determined an effective internal radius (R_i) for Couette geometry which was found to be independent of the nature of the fluid.

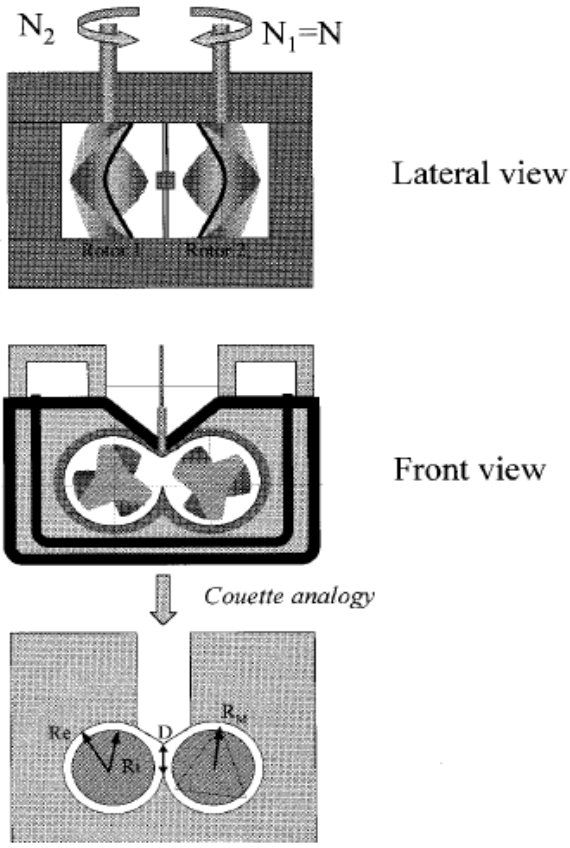

Figure 2.12 Schematic diagram to represent Couette analogy [32]

The expression for calculating the effective radius, shear stress and shear rate given by Bousmina et al. is shown below

$$R_i = \frac{R_e}{\left[1+\frac{4\pi N}{n}\left(2\pi KLR_e^2\frac{1+g^{n+1}}{\Gamma}\right)^{\frac{1}{n}}\right]^{\frac{n}{2}}} \quad \textbf{2.5}$$

$$\tau = \frac{\Gamma}{2\pi r^2 L} \quad \textbf{2.6}$$

$$\gamma = \frac{4\pi N}{n} * \frac{\left(\frac{R_e}{r}\right)^{\frac{2}{n}}}{n\left[\left(\frac{R_e}{R_i}\right)^{\frac{2}{n}} - 1\right]} \quad \textbf{2.7}$$

where R_e is the equivalent radius of mixing chamber, R_i is the effective radius, G is the gear ratio, n is the power law index, N is the rotor speed, and Γ is the torque acting on the cylinder at radius r and length L. The authors showed one way to obtain value of R_i by performing a calibration using either a Newtonian or any power-law fluid at a known torque and rotor speed [33]. This method was tested by many researchers over the years to quantify torque-rotor speed data [34]. They showed the validation of this method even when using different complex geometries and fluids [35].

Another approach used to determine the shear rate and viscosity through the rotational velocity of the impeller is by power consumption method. Metzner and Otto's work on the mixing of non-Newtonian fluids is one of the best-known paper. Their approach is mainly based on a very simple assumption that shear rate is proportional to the impeller speed. It consists of estimating power consumptions of non-Newtonian fluids and then matching it with Newtonian data at the same rotor speed to estimate effective viscosities. In a laminar flow region for a Newtonian fluid, power number and Reynolds are correlated by empirical relationship given below:

$$R_e = \frac{\rho N d^2}{\mu}; \quad \textbf{2.8}$$

$$N_p = \frac{P}{\rho N^3 d^5} \quad \textbf{2.9}$$

Where P is power, N_p is power number, R_e is Reynolds number and N is the rotation of speed of the impeller. The above relation is used to determine power measurements and viscosity by measuring torque (P=2πN*Torque). In case of Power-fluid, the above equation can be used to

calculate apparent viscosity for a non-Newtonian fluid if shear rate is considered average around the impeller.

$$\gamma_{av} = K_s \cdot N; \text{ where } K_s \text{ is Metzner and Otto constant for each impeller.}$$

Based on this idea, Castell et al. demonstrated three viscosity matching methods that can be used to calculate constant K_s. Power Curve method uses power curves of Newtonian and non-Newtonian fluid to calculate viscometry constant. Values of Re are determined using these power curves and then used to calculate viscosity. Torque Curve method uses graphs of torque as a function of impeller rotational speed to calculate slope and then constant. Glenn et al. used another Matching Stress Method to determine viscosity in Pilot scale mixer.

C. Salas-Bringas et al. [15] developed a prototype on-line rheometer to predict viscosity in a continuous manner. This new rheometer was based on the principle of using torque and rotational speed to measure shear rate. They also incorporated additional parameter of power consumption measurements to compare rheological data. However, the authors reported viscosity measurements with an accuracy of ±25 Pa s from the first prototype and proposed to develop more complex models for higher accuracies.

Chapter 3
Experimental Work

The experimental setup and resources used in this study are described in this chapter. The materials used in this experimental work are described in Section 1. In Section 2, equipment and tools used for measurements are described. Then in Section 3, the procedure for emulsions preparation and viscosity measurements are discussed. The following section describes in detail some experimental protocols that were applied to obtain accuracy and reproducibility in this work.

3.1 Materials

The oil used in this study was highly refined white mineral oil obtained from Petro-Canada. Related physical properties are listed in Table 3.1. Experimental grade starch nanoparticles were used to make colloidal dispersions as the aqueous phase. Triton X-100 was used to produce a stable oil-in-water emulsion. Triton X-100 is water soluble and a non-ionic emulsion stabilizer with high HLB value of 13.5. Sodium chloride (99% purity) was purchased from Sigma-Aldrich and used as received.

In the present work, the viscosities were measured with Brookfield LVT viscometer and catastrophic phase inversion was measured using a thermoscientific conductometer (Orion 3-star). For accurate viscosity measurements, two spindles (type YULA-15(E) and LV-1(61)) was immersed in a cylindrical tube chamber, and it is further set to rotate at a given angular velocity. More detail on the operation mechanism of this viscometer will be presented in the subsequent section. Physical Properties of bulk fluids

Table 3.1 Physical Properties of bulk fluids

Bulk Fluids	**Density** (kg/L @ 15°C)	**Viscosity,** (mPa.s @ 21°C)
Purity FG WO 15	0.85	26
Deionized water	992.8	0.98

3.2 Set-up

The experiments were performed in a large mixing tank installed with a rotational viscometer and a homogenizer. Details of the experimental setup is shown in a schematic diagram (**Figure 3.1**) below. The glass tank has a capacity of approximately 20 litres. The dimensions of the tank are: inner diameter = 29 cm; height = 29.5 cm. The system consists of a variable speed Gifford-Wood homogenizer (Model 1-L; Rotor-Stator Type) to prepare emulsion, a viscometer, conductivity probe and UL adapter assembly. The UL adapter spindle consists of a cylindrical spindle which rotates inside the open-ended tube chamber to be used in a tank or a beaker.

3.2.1 Viscosity Measurements

The viscosity characteristics of emulsions were carried out by Brookfield dial viscometer (model LVT) rotated at multiple speed of 60, 30, 12, 6, 3, 1.5, 0.6, and 0.3 rpm. A square speed control knob is used to insure rotation at any required speed. The principle operation of viscometer is to measure the torque required to rotate the spindle immersed in a fluid. For any given viscosity, the resistance or drag is proportional to the rotational speed. Any viscous drag measured by spindle is indicated by deflection of the pointer on a rotating dial connected through a calibrated beryllium-copper spring. Variety of viscosity ranges can be measured by utilizing interchangeable spindles and multiple rotational speeds. For this research work, UL-adapter accessory was attached to rotational viscometer. It consists of a precision cylindrical spindle rotating inside an accurately machined tube. The tube is open ended and thus can be used in a beaker or taken when open. A small diameter spindle (type YULA-15(E) and LV-1(61)) is immersed in the tank to measure the viscous drag of the emulsions at different rotation speeds. Accurate measurements of low viscosity fluids can be made under turbulent conditions. For surfactant stabilized emulsions off-line viscometer (Fann co-axial cylinder viscometer) was used to take viscosity measurements at the high shear rate.

To confirm the repeatability, measurements were repeated at least three times for each dispersed phase concentration. The UL adapter was disassembled before every measurement for proper cleaning of the spindle and stainless-steel tube chamber (figure 3.4). Viscosity

measurements were then taken at different shear rates. In every experiment, emulsions were continuously mixed, and a calculated volume of dispersed phase was added to the known volume of oil-in-water dispersions. The total volume of oil-in-water emulsions were maintained at 11 litres for every case. Thus, the concentration of the dispersed phase is increased by withdrawing the O/W emulsions and simultaneously adding pure dispersed phase to maintain the total volume.

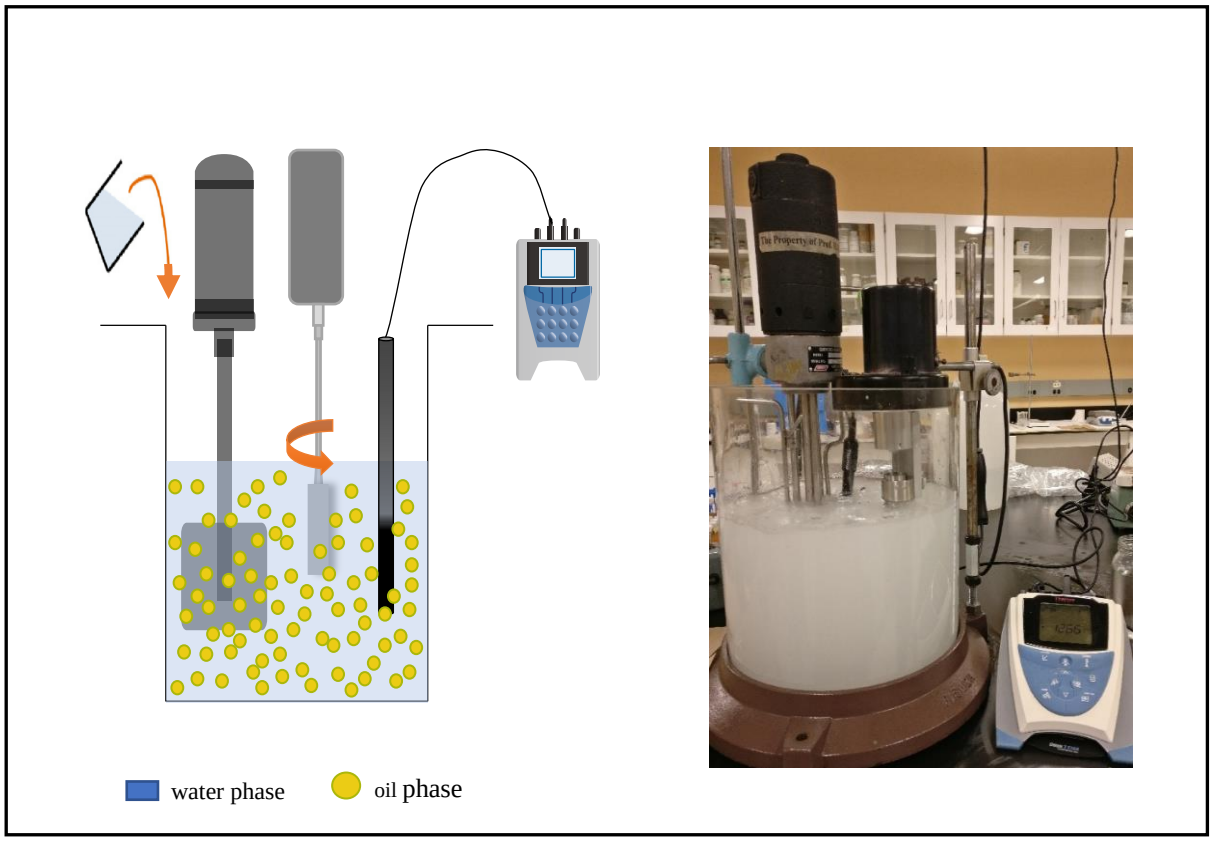

Figure 3.1 Schematic diagram of the experimental setup used for the measurement of viscosity. 1: High Shear Homogenizer; 2: Rotational Viscometer; 3: Enhanced UL adapter spindle; and 4: Conductivity probe

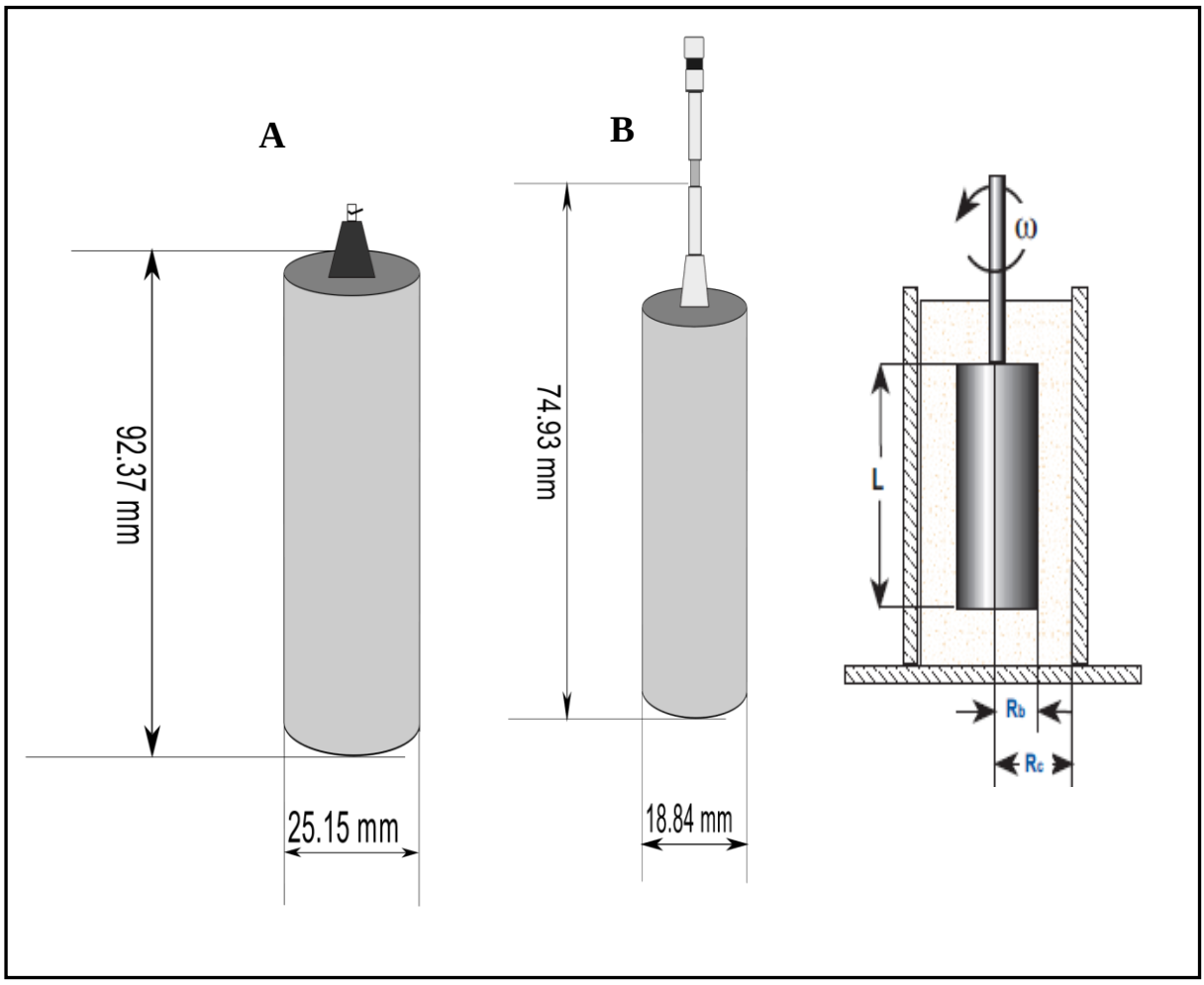

Figure 3.2 Schematic diagram for the YULA-15(E) (A) and LV-1(61) (B) spindle.

Based on the experimental observation, the YULA-15(E) and LV-1(61) are the best spindles to be used for the measurements. YULA-15(E) was used in oil-in-water emulsions experiments and LV-1(61) was used in water-in-oil experiments. Dimensions of the two spindles is shown in a schematic diagram (**Figure 3.3**) above. Table 3.2 gives further information about the measuring system used in this experimental work. Maximum rotation was achieved by using these spindles, obtaining torque values greater than 10% and below 100%. Trial and error method was used for selecting a spindle speed, dial reading between 10

and 100 was obtained was adjusting the speed of the spindle. A higher speed is selected if speed is under 10 and a lower speed is selected if the dial reading is over 100.

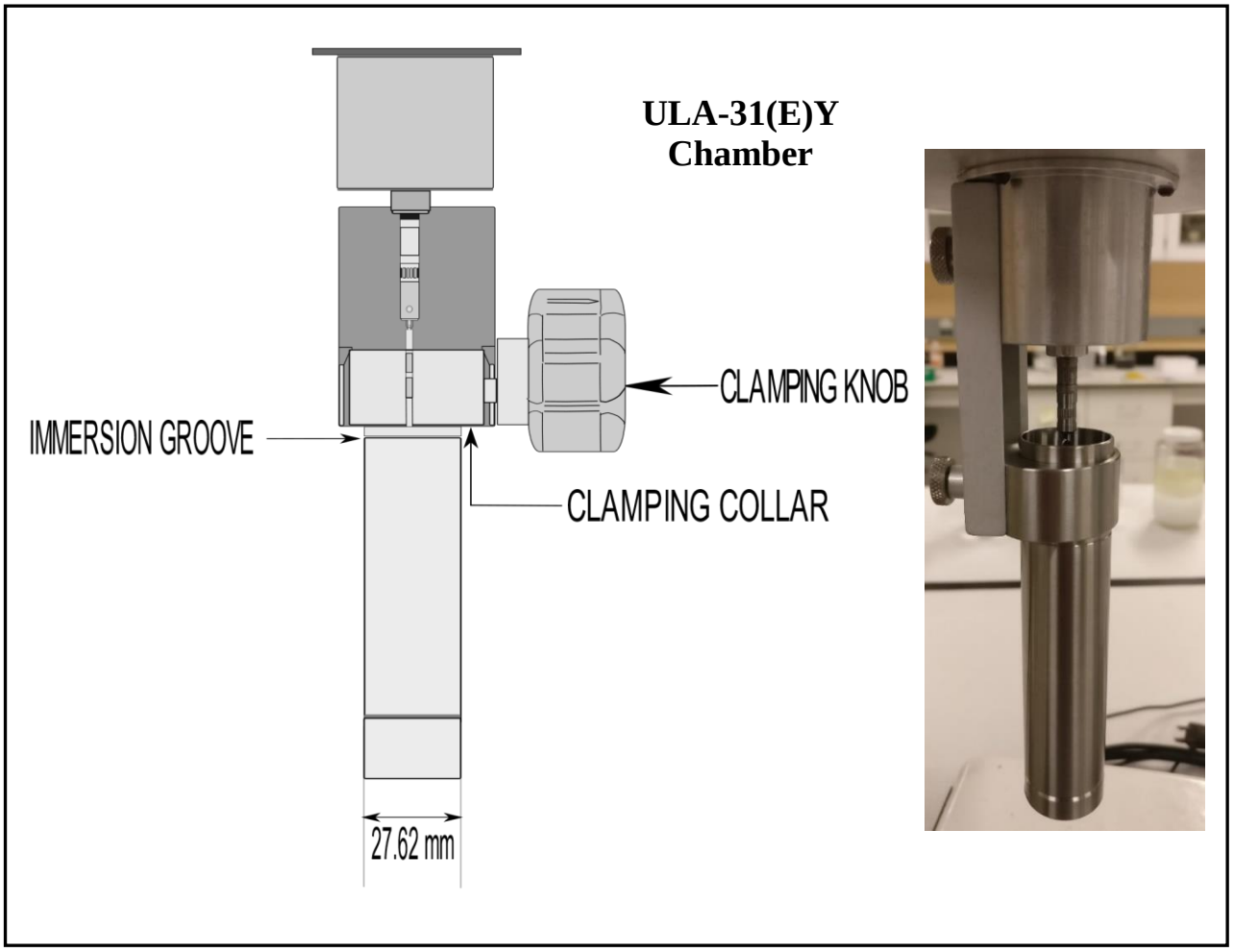

Figure 3.3 Schematic diagram for the ULA-31(E)Y open end sample chamber used for emulsion viscosity measurements.

Table 3.2 Specifications of the measuring system (spindles) used.

Spindle Effective Length	Diameter	Chamber Inside Diameter	Shear Rate (sec^{-1})
3.6366 (92.37)	0.9893 (25.15)	1.0875 (27.62)	1.226N
2.95 (74.93)	0.7417 (18.84)	1.0875 (27.62)	0.391N

Dimensions are in inches(mm) [Source: Brookfield's More Solutions to Sticky Problems] The operating parameters of the spindle geometry are defined by the equations shown below to calculate shear rate and shear stress.

Shear Rate (sec^{-1}): $$\gamma = \left(\frac{2{R_c}^2}{{R_c}^2 - {R_b}^2}\right)\omega \quad \textbf{3.1}$$

Where, $$\omega = \frac{2\pi(rpm)}{60} \text{ (rad/sec)} \quad \textbf{3.2}$$

Shear Stress ($dynes/cm^2$): $$\tau = \frac{M}{2\,\pi\,{R_b}^2 L} \quad \textbf{3.3}$$

Viscosity (poise): $$\eta = \frac{\gamma}{\tau} \quad \textbf{3.4}$$

R_c = radius of container;

R_b = radius of the spindle;

M = torque input by the instrument (673.7 dyne-cm or 0.063 milli-Newton-m);

L = effective length of the spindle.

Substituting the standard dimensions of viscometer, one may obtain from the following equation the shear rate which is used to calculate viscosity.

3.2.2 Microscopy

A Zeiss optical microscope connected to a computer was used to take photomicrographs of all sets of emulsions samples. A small quantity of a prepared emulsion sample was diluted with the same continuous phase and was placed on a glass slide. Droplet were then analyzed with ImageJ software.

3.3 Preparation of Starch Nanoparticle Dispersions

The nanoparticle dispersions were prepared by slowly sprinkling calculated amount of wt% SNPs into a 0.01 mol/L NaCl solution used an aqueous phase and ensuring no clumps of

particles during dispersions. The sole purpose NaCl was added to increase the conductivity of the solution. For better mixing conditions and faster dispersion high shear Gifford-Wood homogenizer (model 1-LV) is used. To ensure complete dissolution, the solution was homogenized at 60 volts for a duration of 60-90minutes at room temperature 22° ± 2°C. Mixing time depends on the amount of nanoparticles. The dispersions were brought to room temperature before they could be used in the emulsification experiments.

3.4 Preparations of Emulsions

In this study, three different types of oil-water-particle emulsions solutions were prepared using the homogenizer. Surfactant-stabilized oil-in-water emulsions were prepared by adding 0.5% (by volume) Triton X-100 surfactant in the aqueous phase and then slowly adding oil of known volume as the dispersed phase. Nanoparticles-stabilized O/W and W/O emulsions were prepared by sequentially adding white mineral oil as the oil phase and SNPs dispersion as the aqueous phase. The solution was continuously sheared during and after the addition of dispersed phase. All rheological measurements were made after 10 minutes of homogenous mixing, and this step was repeated after every dispersed phase volume. Homogenizer was carefully controlled to achieve maximum shearing and minimal air entrainment. After a couple of trial runs, optimum speed of 60 volts was chosen and maintained throughout the experiment. A typical emulsion experiment is as follows: aqueous phase (SNPs dispersion with NaCl) was prepared with deionized water. Depending upon the type of emulsion, 11 litres of either phase (oil or water) was then transferred to the tank. A known amount of dispersed phase was then added to the solution and continuously mixed using a variable speed homogenizer.

3.5 Accuracy and Reproducibility

Brookfield viscometers are designed to be accurate to within ± 1% of the full-scale range of the spindle/speed combination in use. A lot of variables, such as viscometer and spindle type, sample container size, sample temperature, bulk fluids used and the emulsion sample preparation technique, all contribute to affect the accuracy of viscosity measurements.

To prevent errors, those variables were kept constant during each set of measurement. When making a viscosity measurement rotation speed, spindle type, temperature and time of measurement should always be recorded. Homogeneity of the fluid is also important in the case of the unstable emulsion system. In this experiment, the effect of emulsion separation during the measurement was estimated. The whole solution was mixed homogenously for 10 minutes before any set of measurements.

For each concentration, three sets of measurements were taken to ensure the accuracy and reproducibility of the readings. Readings were also recorded as a function of time as the spindle was rotating inside the chamber to investigate any effect of separation on the viscosity measurements. Also, before every set of measurements, UL adapter assembly was disassembled and cleaned and then immersed again into the solution.

Chapter 4
Results and Discussion

This chapter discusses experimental results in detail obtained in this study. Section 4.1 discusses the rheology of oil-in-water (O/W) emulsions in the presence of surfactant stabilizer and solid nanoparticles, separately. The in-line and offline viscosity results from this investigation were used to compare and understand the behaviour of two systems. Section 4.2 describes the experimental results for water-in-oil (W/O) emulsion at different starch nanoparticle concentrations.

4.1 Oil-in-Water Emulsions

This section presents experimental results on the comparative study done between oil-in-water emulsions prepared using Triton X-100 and starch-nanoparticles. The rheology of the O/W emulsions prepared with 0.5% (v/v) surfactant was studied prior to nanoparticles. For comparison purposes, it felt necessary to study in-line and offline viscosity data of surfactant-stabilized emulsions. The second objective of this study was to understand and eliminate various factors leading to the wrong and misleading interpretation of viscosity data while making in-line measurements. The experimental procedure consisted of acquiring, at the same time, the rheological profile of surfactant-stabilized emulsions at same temperature from both on-line and offline instruments.

Viscosity data for emulsions with solid-nanoparticles behaved in a different manner to the data for emulsions with a surfactant. Emulsions with nanoparticles were unstable, especially with increasing dispersed phase volume and required continuous mixing. As a result, offline viscosity measurement was not possible in the case of the unstable starch nanoparticles emulsion system. Hence, the on-line viscosity measurement system delivers the solution to the above problem and, also provides continuous real-time monitoring.

4.1.1 Surfactant-Stabilized Emulsion

Figure 4.1 shows the plot of in-line viscosity data for surfactant-stabilized O/W emulsions. The oil concentration was varied up to 70% by volume. It is seen that emulsion viscosity increases considerably with the increase in the volume of the dispersed phase (oil). The slopes of the straight lines are different depending upon the oil concentrations. The shear viscosity of the starch nanoparticle were measured as a function of shear rate for dispersed phase volume concentration. The flow curves of starch nanoparticle can be fitted to a power law model as:

$$\tau = K\gamma^{n} \text{ or } \eta = K\gamma^{n-1}$$

In the above equation, the power law model is described by two parameters, where K and n are power law constant, τ the shear stress, γ is the shear rate and η is the apparent viscosity. When the slope (power law index) is unity, the fluid shows a Newtonian behaviour and when n is less than unity, emulsions are pseudoplastic fluids.

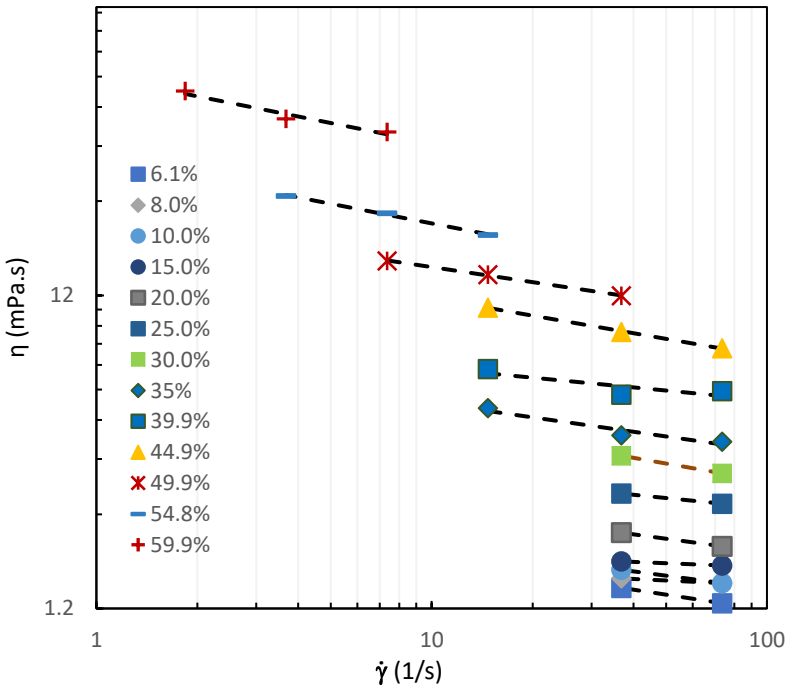

Figure 4.1 Viscosity vs. Shear rate for surfactant stabilized emulsions obtained using the In-line Viscometer.

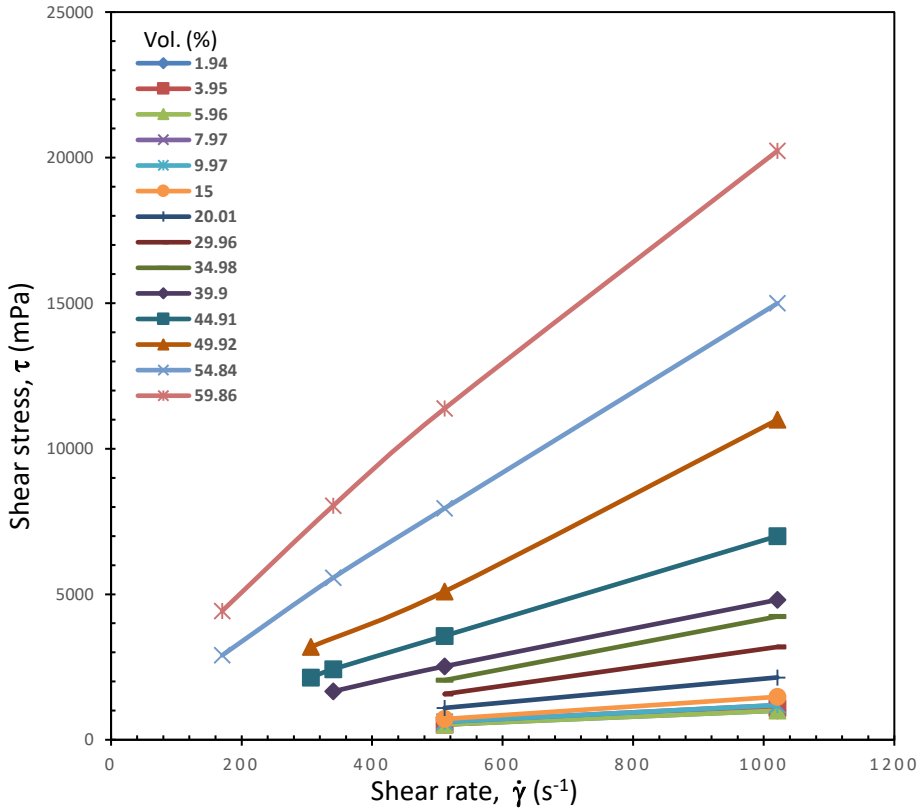

Figure 4.2 Shear stress vs. Shear rate for surfactant stabilized emulsions obtained using the offline Viscometer.

Figure 4.1 shows the rheogram of the emulsions, i.e. log η vs log γ plots. The slopes of the straight lines are different, depending on the oil concentration. Figure 4.2 shows the viscosity data for surfactant-stabilized emulsions obtained with offline instrument-Fann 35. Fann-35 operates at a higher RPM than Brookfield viscometer, so the offline viscosity data was collected at high shear rates. The O/W emulsions are Newtonian upto a dispersed-phase (oil) concentrations of 35% by volume. At higher concentrations of water, the O/W emulsions displayed non-Newtonian shear thining behaviour similar to that obtained with online measurements. It is interesting to note that the in-line viscometer covers the low shear rate region whereas the offline viscometer covers the high shear rate range.

Figure 4.3 presents a combined viscosity data the plot obtained from both in-line and off-line measurements. It is clear from plot that both offline and in-line measurements complement each other.

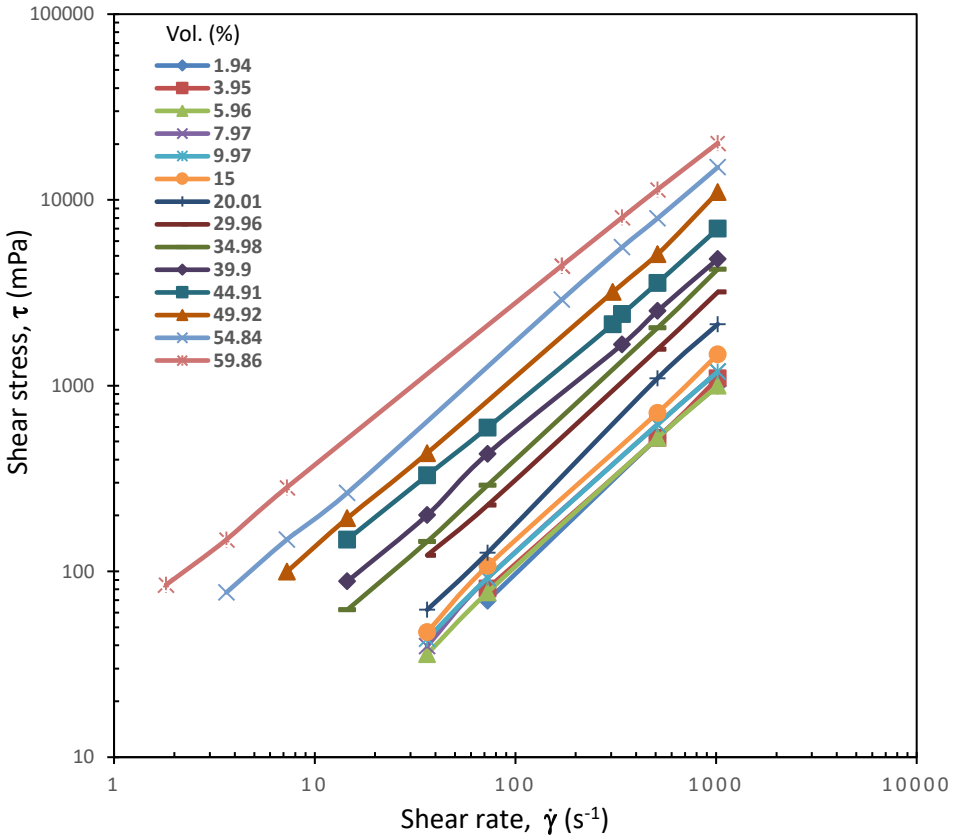

Figure 4.3 Combined viscosity data for surfactant stabilized emulsions obtained using the on-line (low shear rate) and offline (high shear rate) Viscometers.

4.1.2 Solid Nanoparticles-Stabilized Emulsions

Figure 4.4 shows the rheological properties of nanoparticles-stabilized emulsions on the basis of shear stress versus shear rate relationship. Emulsions were prepared by adding oil (dispersed phase) into 2 wt.% nanoparticles dispersions (continuous phase). The data was collected for various value of dispersed phase concentration. At low oil concentrations (1.9%~25% by volume, respectively), emulsion exhibit Newtonian Behaviour. With further

increasing oil concentrations, the viscosity of emulsions decreases with an increase in shear rate. Emulsions are non-Newtonian at higher oil concentrations, particularly at 70% by volume of oil.

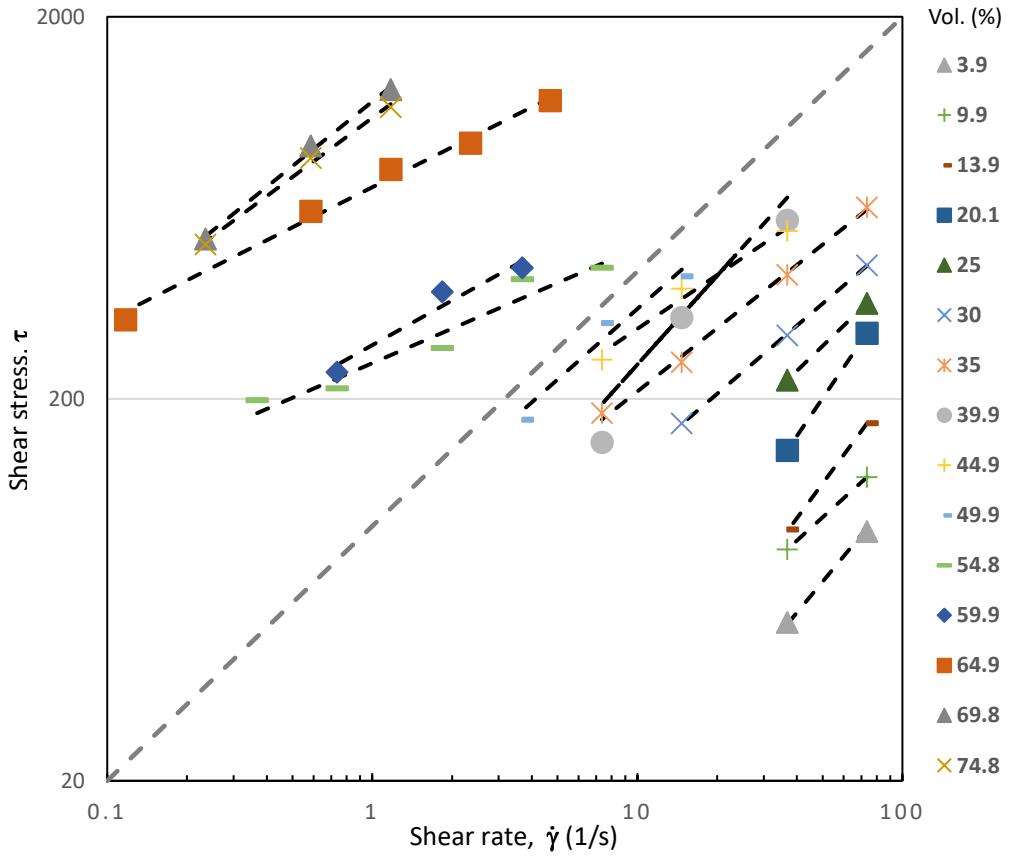

Figure 4.4 In-line Visocosity data for starch-nanoparticle oil-in-water emulsions.

Viscosity shows the dramatic increase from 50% O/W to 50% O/W and then again from 60% O/W to 65% O/W emulsion. For comparison purposes, the results of the power law constants are reported in Table 4.1. Even visual observations made during experiment indicated the importance of particle interactions at high dispersed-phase concentrations. In the present study, the maximum value of the apparent viscosity is around an oil volume percent of 50% as shown in figure 4.4. Thus, in the following experiment, we investigate on rheological characteristics of the emulsions at this point. Knowledge of the droplet of the dispersed phase and its polydispersity is important in characterizing emulsion stability and improving the understanding of the emulsification process.

Table 4.1 Values of shear-thinning index and consistency index for surfactant and nanoparticles-based emulsions

Surfactant-stabilized oil-in-water emulsions											
Concentration (vol.%)	**6.1%**	**8.0%**	**10.0%**	**20%**	**25%**	**30%**	**35%**	**39.9%**	**44.9%**	**54.8%**	**59.9%**
k	2.51	2.65	1.98	3.52	4.10	7.24	7.73	18.06	21.35	32.90	60.18
n	0.83	0.85	0.95	0.85	0.89	0.81	0.84	0.81	0.84	0.79	0.78

Starch nanoparticles-stabilized oil-in-water emulsions													
Concentration (vol.%)	**3.9%**	**9.9%**	**13.9**	**20.1%**	**25%**	**30%**	**35%**	**39.9%**	**44.9%**	**49.9%**	**54.8%**	**59.9%**	**64.9%**
k	2.51	8.39	0.86	3.74	20.05	34.82	58.90	41.43	103.79	83.61	247.86	2776.36	715.89
n	0.83	0.62	1.23	1.01	0.66	0.59	0.55	0.77	0.46	0.61	0.30	0.38	0.34

Conductivity and temperature readings were also recorded to test whether the O/W emulsions exhibited any catastrophic phase inversion behaviour. Figure 4.5 shows the course of the conductivity and temperature at a different volume percent of dispersed phase during the experiments. As seen in figure 4.5, experimental data decreases exponentially as the concentration of the dispersed phase (oil) is increased. This observation suggested that phase inversion did not occur at any volume concentrations which is in agreement with the viscosity results. No external heat was supplied during the experiment. However, mechanical mixing by homogenizer did varied the temperature between 22 °C and 28 °C.

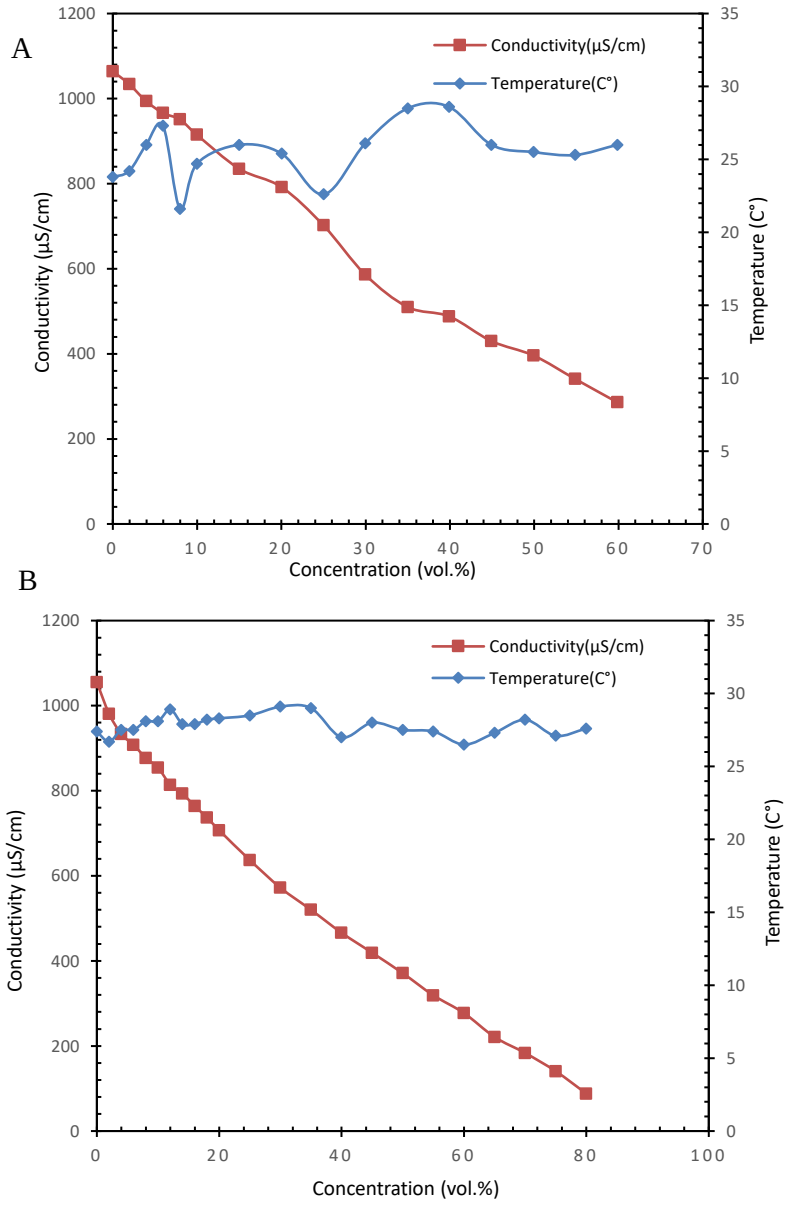

Figure 4.5 Conductivity and temperature course during the experiment. A) O/W emulsion with a surfactant; B) O/W emulsion with solid-nanoparticles.

4.1.3 Emulsion Stability

Emulsion stability was examined for O/W emulsions prepared from individual surfactant and solid-nanoparticles. Oil-in-water emulsions (50% v/v) were prepared using 0.5% (by volume) Triton X-100 and 2% wt. solid-nanoparticles. The stability of emulsions was monitored over a period of two weeks and was determined by visual observation. Photographs of the emulsions formed were taken at different time intervals to study the effect of phase separation.

Figure 4.6A-C shows the images of emulsions at three different stages during phase separation. Nanoparticle-stabilized emulsions creamed faster than the surfactant stabilized emulsions. After two weeks, surfactant emulsions showed little change except for gravitational creaming at the bottom. On the other hand, O/W emulsions with nanoparticles droplet grew bigger over time and showed noticeable phase separation as shown with a magnified view of figure 4.6-C. After the first stage, emulsions stabilized using surfactant remained at a consistent appearance over a period, indicating a stable emulsion. Emulsion creamed into two distinct layers: a large top layer that was brighter white and cloudy and a bottom layer that was white and cloudy. Separated surfactant-emulsions can be recreated by simply shaking the solution or by providing a very low energy input. In contrast, nanoparticles-stabilized emulsions creamed into the two-layer system: the large top layer was cloudy which appeared to be a collection of aggregated droplets followed by slightly cloudy bottom layer. This behavior of phase separation and droplet coalescence shown by nanoparticle-stabilized emulsions was supported further by comparing droplet sizes thorough microscopy.

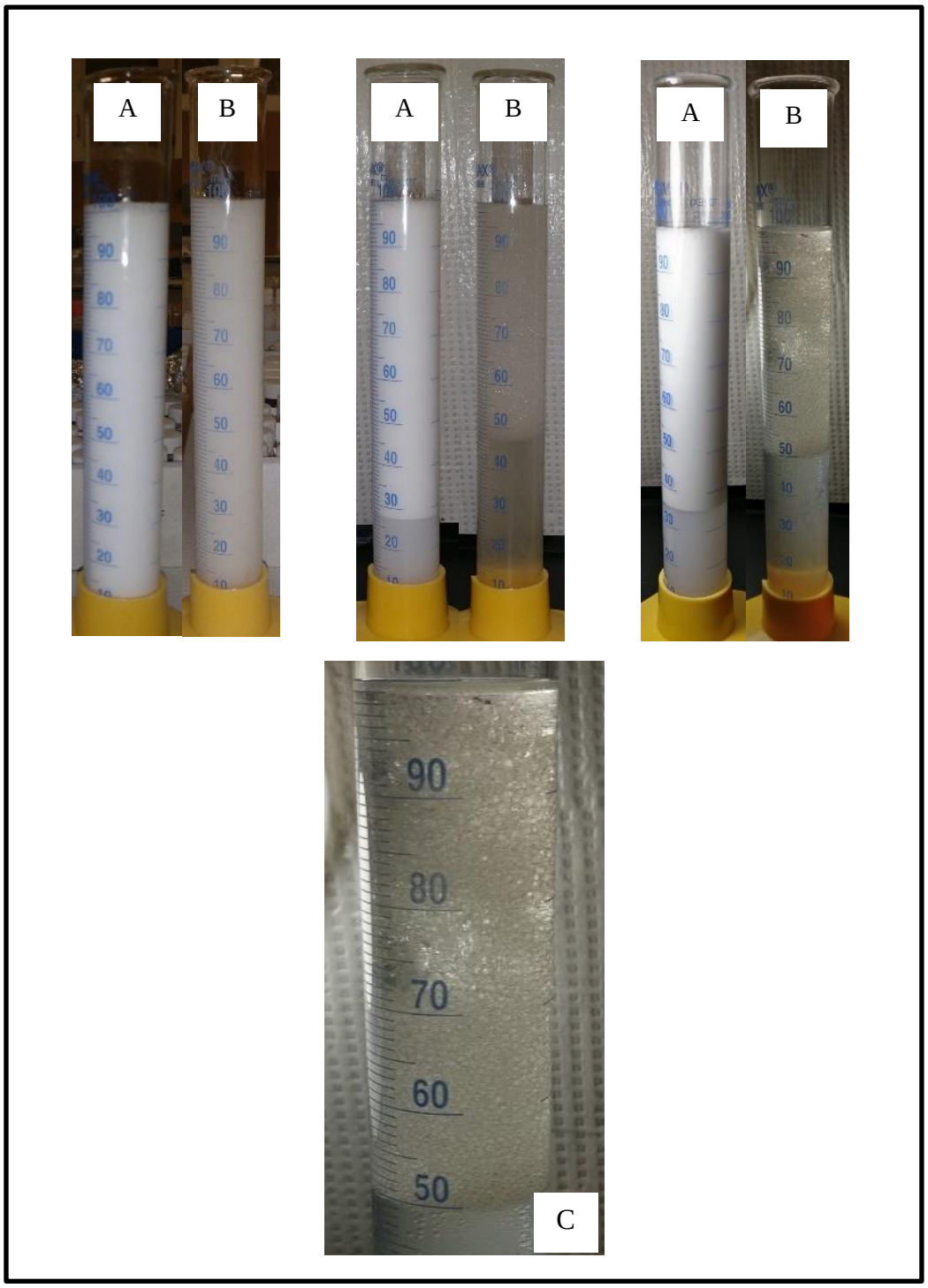

Figure 4.6 Photographs of O/W emulsions in graduated cylinder produced with A) 0.5% (by volume) Triton X-100 surfactant; B) 2% wt. solid-nanoparticles; C) Magnified view of phase separation in nanoparticle emulsion system.

4.1.4 Microscopy

The photomicrographs for the oil-in-water emulsions of surfactant (A) and nanoparticle (B) are shown in Figure 4.7-8, respectively. These two sets of emulsions were prepared having an oil volume concentration (dispersed phase) of 50%. These emulsions were then diluted with same continuous phase or DI water before taking the photomicrographs. Clearly, the droplets of the surfactant emulsions are much smaller than the droplets of the corresponding nanoparticles emulsions as seen in figure 4.9. Emulsions with a very narrow range of droplet size distribution were produced by surfactant. The Sauter mean diameters of the surfactant and nanoparticles emulsions are 14 and 91 µm, respectively.

Microcopy of surfactant- and nanoparticles-stabilized emulsions were monitored over a period of 24 hours to study the effect on emulsions stability and droplets size distribution. Droplets stabilized by surfactant were perfectly spherical with fine droplets and few large ones with diameters up to approximately 90 µm (Figure 4.7). The optical micrographs of solid-nanoparticles stabilized emulsions were different from surfactant-stabilized emulsions (Figure 4.8). Clearly, the droplet size of the surfactant-emulsion is much smaller than that of the nanoparticle-emulsion.

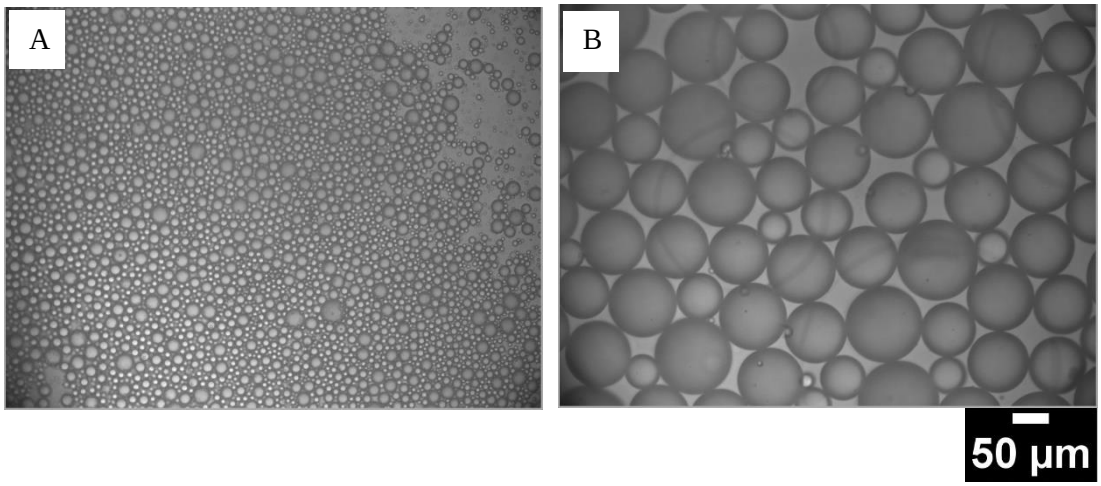

Figure 4.7 Comparison of droplet size at t =0. (A) Surfactant-stabilized emulsions; (B) Solid nanoparticles emulsions.

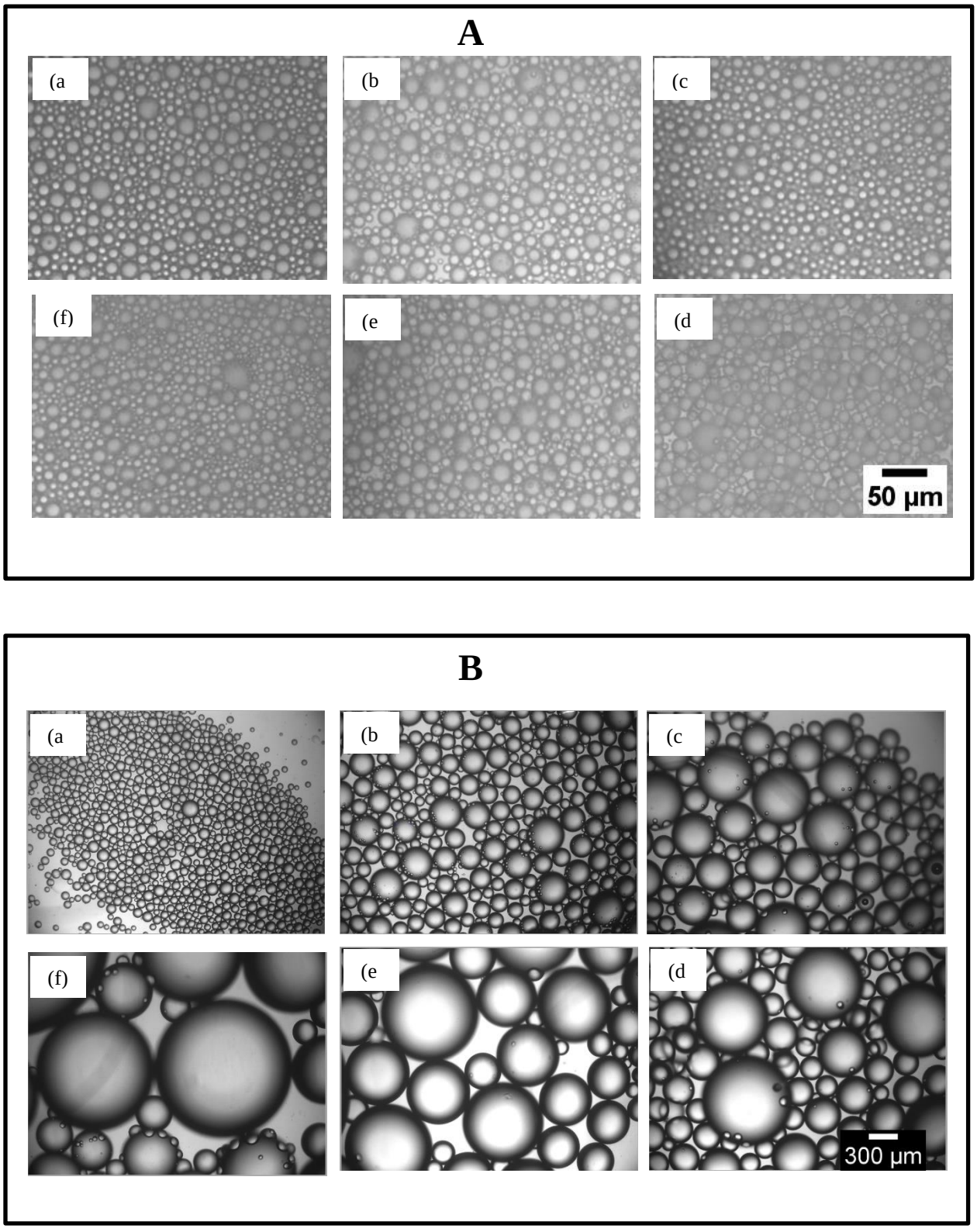

Figure 4.8 Optical micrographs of O/W emulsion stabilized by Triton X-100 (A) and nanoparticles (B) at different time intervals. (a) t=0, (b) t=1hr, (c) t=3hr, (d) t=5hr, (e) t=8hr, (f) 24hr.

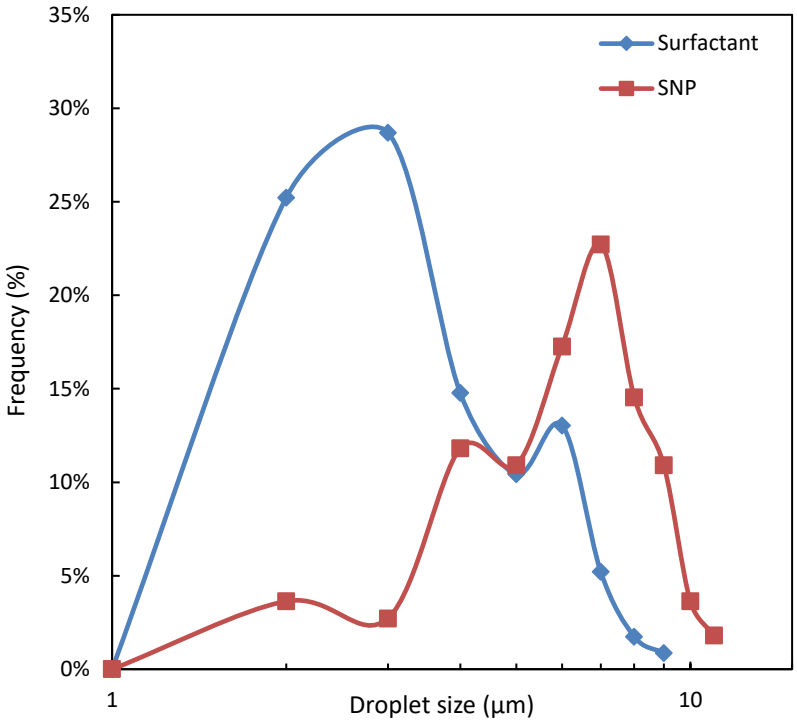

Figure 4.9 Comparison of the droplet size distribution between nanoparticle and surfactant

Emulsions were left to age at room temperature and microphotographs were taken at various intervals during this time. Figure 4.7 and 4.8 compares the effect of aging on droplet size and droplet size distribution over a period of 24 hr. Microscopic observations indicated significant changes for nanoparticle- stabilized emulsions. Triton-stabilized emulsions remained at a consistent size of approximately 14 µm over the 24-hour period, indicating a stable emulsion. The nanoparticle-stabilized emulsion droplet size increased from 25 to approximately 150 µm in 24-hour time. Figure 4.10 shows the evolution in mean droplet size as a function of time for oil-in-water emulsion stabilized with surfactant and starch nanoparticles.

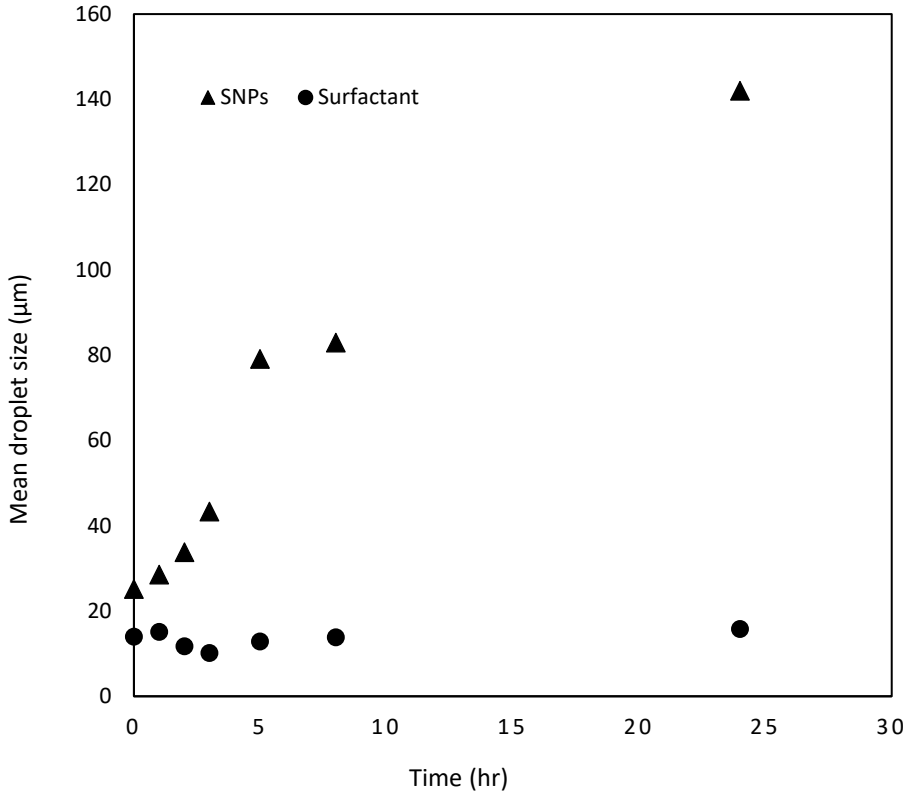

Figure 4.10 Mean droplet size as a function of time.

4.2 Water-in-Oil Emulsions

In this work, the In-line viscosity data for water-in-oil (W/O) emulsions prepared using different nanoparticles concentrations are studied. The W/O emulsions showed catastrophic phase inversion affected by nanoparticles concentration and dispersed phase volume fraction discussed in subsequent sections. Also, the influence of nanoparticles concentration on emulsion stability was investigated before and after phase inversion.

4.2.1 Emulsion Preparation

Water-in-oil emulsions were produced by using starch nanoparticles dispersions as the dispersed phase and oil as the continuous phase. The aqueous nanoparticles dispersions were

prepared by slowly adding the calculated amount of nanoparticles into 0.01M NaCl solution. The sole purpose of NaCl was to enhance the conductivity of the system. Note that the same concentration of salt was used throughout the experimental work. The agitation was continued until the nanoparticles were dissolved completely resulting in a clear solution. The starch nanoparticle concentration was varied from 0.25% to 2% (by weight) based on the aqueous phase. The emulsions of the water-in-oil type were prepared at room temperature by sequentially adding dispersed phase (nanoparticles dispersions) into the continuous phase (oil). To produce stable emulsions, continuous mixing and shearing was provided by a variable speed homogenizer.

4.2.2 0.25% nanoparticles dispersion *(concentration by wt.)*

Figure 4.10 shows the relation between shear stress and shear rate for water-in-oil (W/O) emulsions. The emulsions were prepared using 0.25% by weight concentration of nanoparticles solution. The data is shown for different volume percent of nanoparticle dispersions. The viscosity of W/O emulsion increases with increasing dispersed phase volume before reaching phase inversion point, beyond which the water becomes the continuous phase.

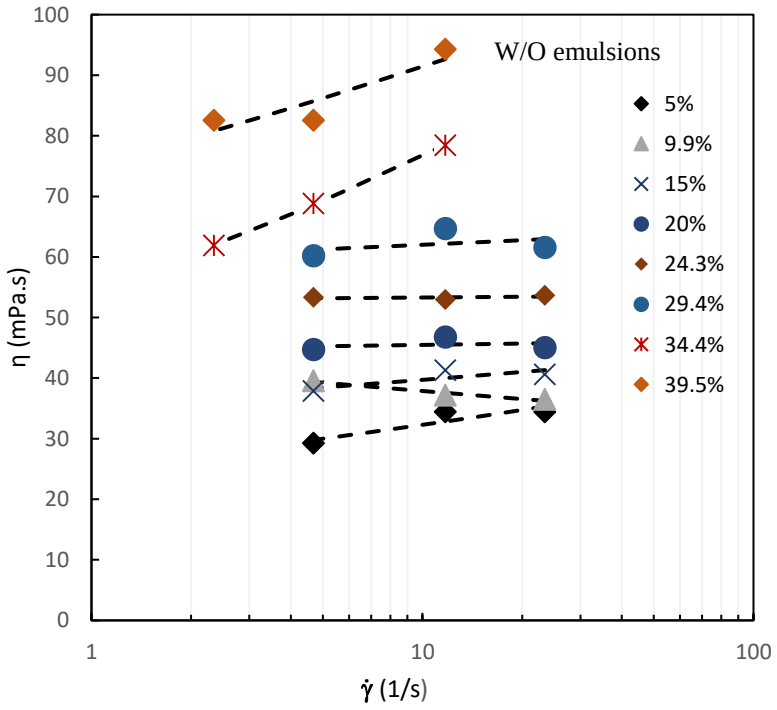

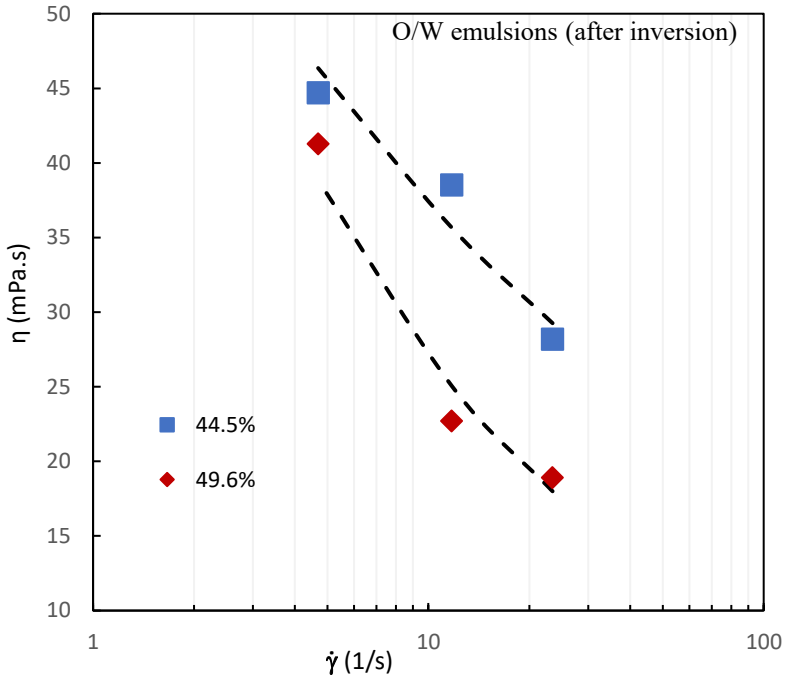

Figure 4.11 Rheograms for 0.25% wt. nanoparticles emulsion at different dispersed phase volume concentration.

From the above plot following observations can be made:

1) As the concentration of aqueous dispersions is increased, emulsion shows a shear thinning (non-Newtonian) behaviour. A further increase in dispersed phase resulted in phase inversion reported by both viscosity and conductivity readings.
2) Clear phase inversion is seen to occur around 44.5% of dispersed phase volume. Emulsions changes from water-in-oil emulsions to oil-in-water emulsions.
3) After phase inversion, emulsions viscosity decreases drastically. As the water becomes the continuous phase, the non-Newtonian behaviour is still observed.

4.2.3 0.5% nanoparticle dispersion (*concentration by wt.*)

Figure 4.10 shows the variation of shear stress with shear rate for W/O emulsions prepared using 0.5% by weight NPs solution. Dispersed phase (nanoparticles) concentration was varied up to 54.6% by volume. Emulsions showed similar behaviour as in 0.25% wt. NPs

emulsion and acted as Newtonian till 44.5% volume of water. The flow curves shift to higher shear stress with the increase in the aqueous concentration. The viscosity increases with the increase in the concentration of the nanoparticles.

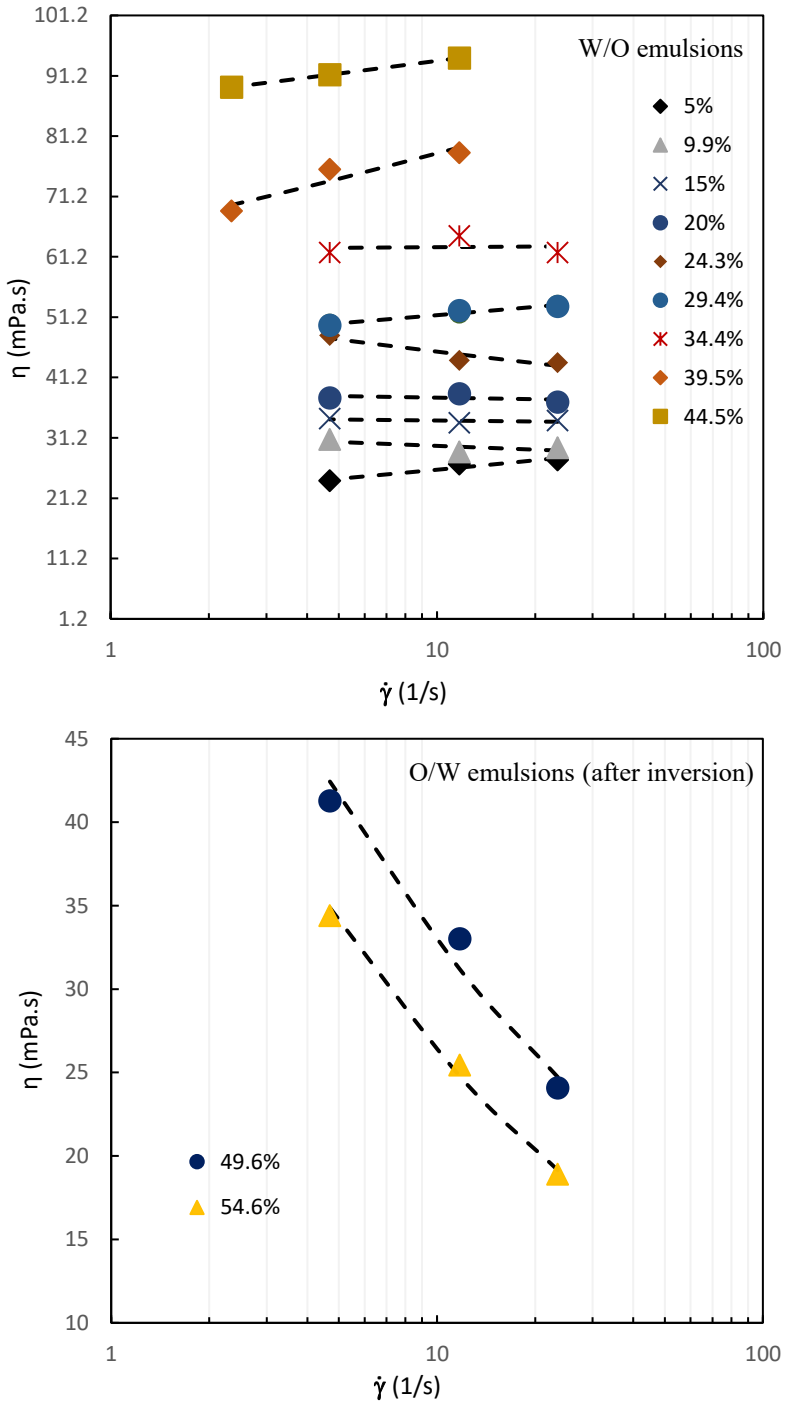

Figure 4.12 Viscosity vs. Shear rate for 0.5% wt. NPs emulsion at a different volume of the dispersed phase.

Also, a stronger shear thinning behaviour is seen with the increase in the nanoparticle concentration in the aqueous phase. Phase inversion took place at a slightly higher concentration as compared to the previous experiment. At a water concentration of 49.6% volume, a sudden decrease in the viscosity occurs due to phase inversion of water-in-oil emulsion to oil-in-water emulsion.

4.2.4 1% nanoparticle dispersion (*concentration by wt.*)

In Figure 4.11, data shown is plotted for the emulsions prepared from 1% by weight nanoparticle in the aqueous phase. Trends similar to the previous emulsion are observed for a higher concentration of nanoparticle dispersion. Increasing the NPs concentration raises the phase inversion concentration. The phase inversion point shifts from about 49.6 vol.% to over 59.6% vol.% upon increasing the nanoparticle concentration from 0.5 to 1 wt%.

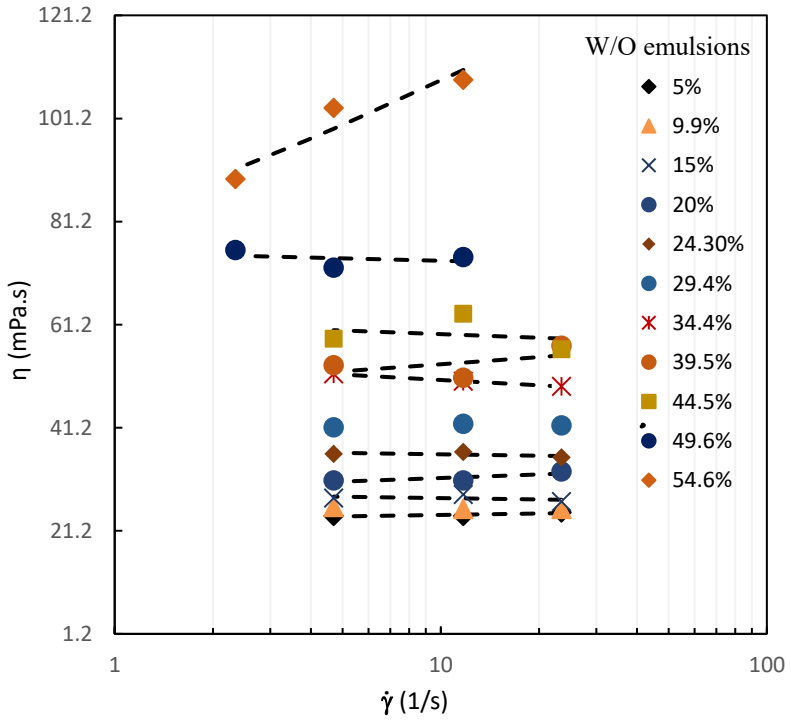

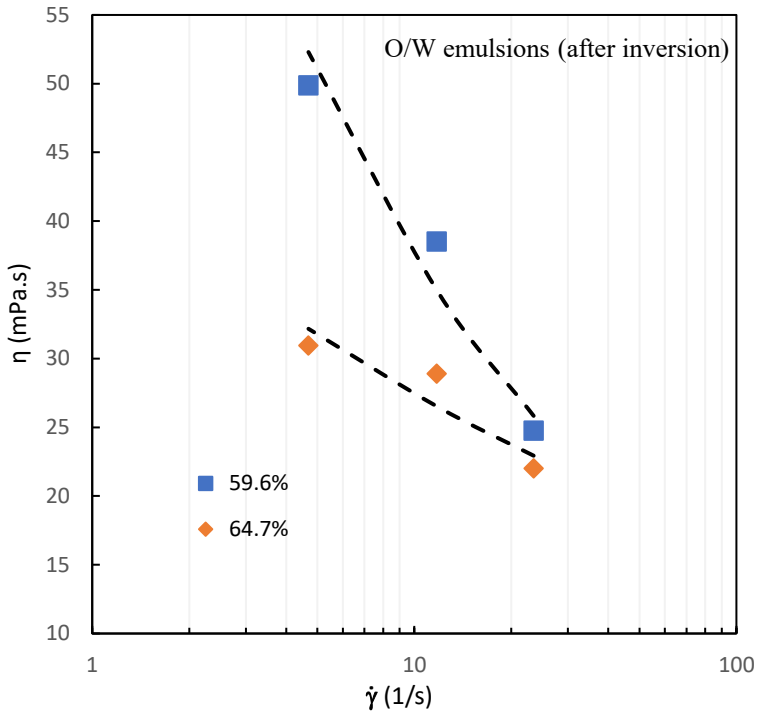

Figure 4.13 Flow curves for 1% wt. NPs emulsion at different volume fraction

4.2.5 2% nanoparticle dispersion (*concentration by wt.*)

Figure 4.12 shows the viscosity of the water-in-oil emulsion. The viscosity of emulsions increases with the increase in the dispersion volume concentrations until phase inversion occurs. For any given volume percent of the dispersed phase and shear rate, the viscosity of emulsions is higher than that of the emulsions with lower nanoparticle concentration in the dispersion. The emulsions were water-in-oil (W/O) type up to a dispersed phase concentration of 59.6% by volume. With a further increase of dispersed phase, the W/O emulsion inverted to an oil-in-water emulsion. A sudden decrease in viscosity is recorded at this point. This transition change was also reported by conductivity readings confirming phase inversion. From the figure, it is seen that after inversion, oil-in-water emulsion exhibit non-Newtonian behaviour. Table 4.2 summarizes details of rheological parameters of power law model for all the concentrations of starch nanoparticles.

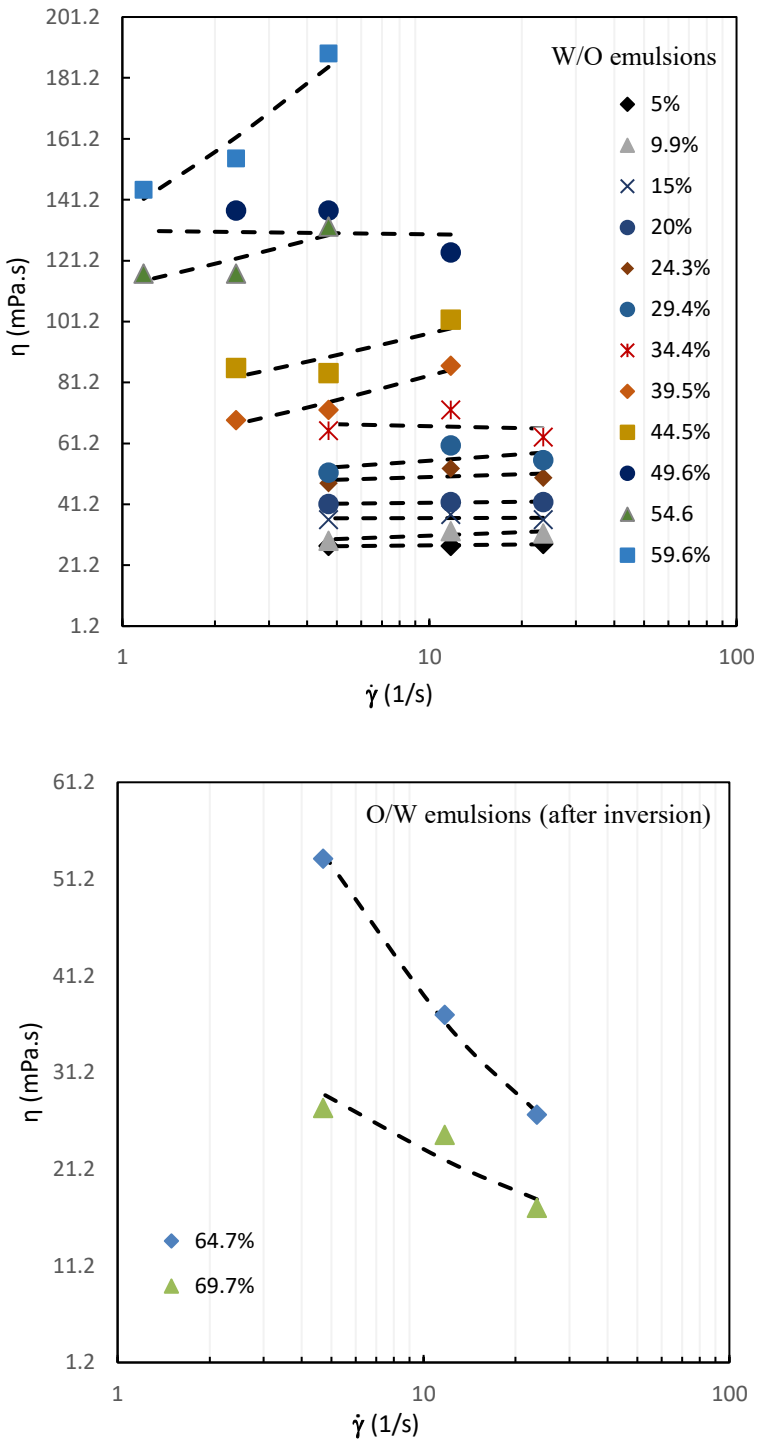

Figure 4.14 Viscosity vs. Shear rate for 2% wt. NPs emulsion at a different volume fraction

Table 4.2 Power law model fitting parameters for starch nanoparticles water-in-oil emulsions

0.25 wt.% starch nanoparticles										
Concentration (vol.%)	**5.0% w/o**	**9.9% w/o**	**15% w/o**	**20% w/o**	**24.3% w/o**	**29.4% w/o**	**34.4% w/o**	**39.5% w/o**	**44.5% o/w**	**49.6% o/w**
k	25.27	42.62	35.66	44.74	52.88	59.56	54.70	75.16	72.11	81.36
n	1.10	0.94	1.04	1.00	1.00	1.01	1.14	1.08	0.71	0.52

0.5 wt.% starch nanoparticles											
Concentration (vol.%)	**5.0% w/o**	**9.9% w/o**	**15% w/o**	**20% w/o**	**24.3% w/o**	**29.4% w/o**	**34.4% w/o**	**39.5% w/o**	**44.5% o/w**	**49.6% o/w**	**54.6% o/w**
k	21.28	32.04	34.63	38.73	52.48	47.18	62.44	65.44	86.85	71.27	61.98
n	1.08	0.96	0.99	0.99	0.93	1.03	1.00	1.07	1.03	0.66	0.62

1 wt.% starch nanoparticles													
Concentration (vol.%)	**5.0% w/o**	**9.9% w/o**	**15% w/o**	**20% w/o**	**24.3% w/o**	**29.4% w/o**	**34.4% w/o**	**39.5% w/o**	**44.5% o/w**	**49.6% o/w**	**54.6% w/0**	**59.6% o/w**	**64.7% o/w**
k	23.36	26.10	28.41	29.22	36.94	41.04	54.02	49.13	61.74	75.14	82.54	102.95	44.51
n	1.01	0.99	0.98	1.03	0.98	1.00	0.97	1.03	0.98	0.99	1.11	0.56	0.78

2 wt.% starch nanoparticles														
Concentration (vol.%)	**5.0% w/o**	**9.9% w/o**	**15% w/o**	**20% w/o**	**24.3% w/o**	**29.4% w/o**	**34.4% w/o**	**39.5% w/o**	**44.5% o/w**	**49.6% o/w**	**54.6% w/o**	**59.6% w/o**	**64.7 o/w**	**69.7% o/w**
k	26.80	27.35	36.44	40.68	47.21	48.88	68.99	59.65	75.67	131.03	112.96	137.1	104.28	45.55
n	1.01	1.05	1.00	1.01	1.02	1.05	0.98	1.14	1.10	0.99	1.08	1.19	0.57	0.70

4.3 Detection of Phase Inversion Points

Phase inversion points can be detected by measuring conductivity and viscosity. To record conductivity and temperature reading during dispersion process, a conductivity probe was placed into the tank. Viscosity at different concentrations is plotted on the single shear rate. All graphs show agreement on transition points of conductivity and viscosity change during phase inversion. Conductivity curve shows an abrupt increase which corresponds to the phase inversion point, whereas at a constant shear rate a drop-in viscosity is seen when water becomes the continuous phase.

In this study, the aqueous phase was varied from 5% to 80% by volume in 5% increments. As the aqueous phase is increased emulsion shows increase in viscosity. The viscosity of emulsion further decreases as the concentration of water is increased. This sudden decrease in viscosity was due to phase inversion. Figure 4.13 illustrates the plots of conductivity and the viscosity, as a function of dispersed phase concentration. When the concentration of the nanoparticles is 0.25 wt.%, the phase inversion occurs at a volume concentration around 44.6 vol.%. As the particle concentration is varied from 0.25 wt% to 0.5 wt%, the phase inversion is delayed from 44.6 vol.% to 49.6 vol.%. A similar trend is observed on further increasing the particles concentration. The phase inversion points for 1 wt.% and 2 wt.% is shifted from 59.6 vol.% to 64.7 vol.%. Viscosity data is shown at the same shear rate for all the plots.

(a)

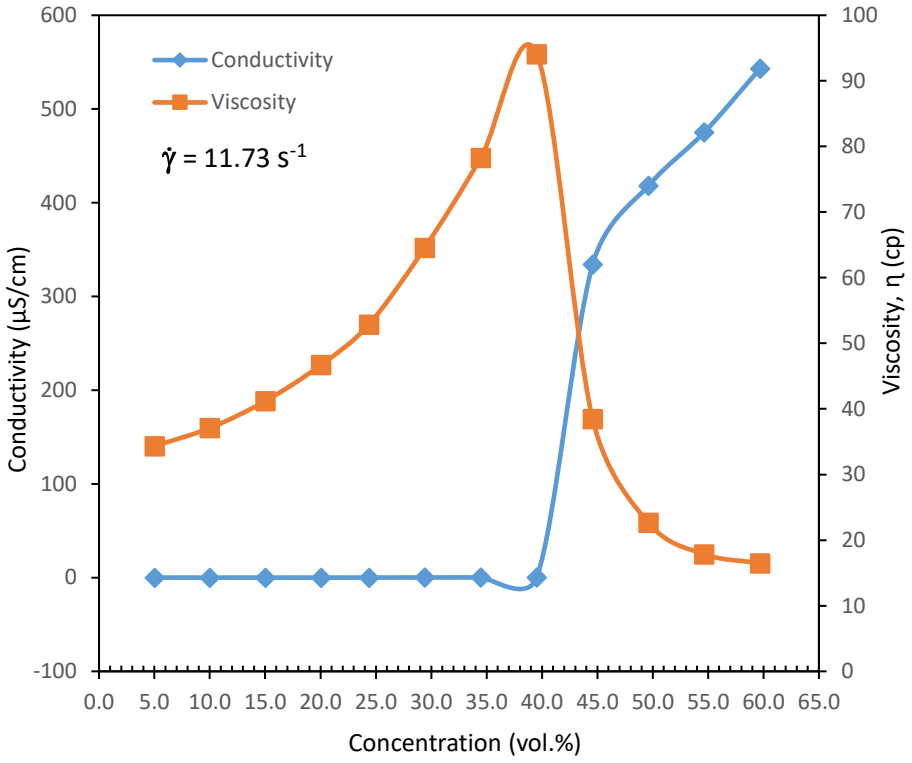
Conductivity
Viscosity
$\dot{\gamma}$ = 11.73 s^{-1}
Conductivity (µS/cm)
Viscosity, η (cp)
Concentration (vol.%)
600
500
400
300
200
100
0
-100
100
90
80
70
60
50
40
30
20
10
0
0.0
5.0
10.0
15.0
20.0
25.0
30.0
35.0
40.0
45.0
50.0
55.0
60.0
65.0

(b)

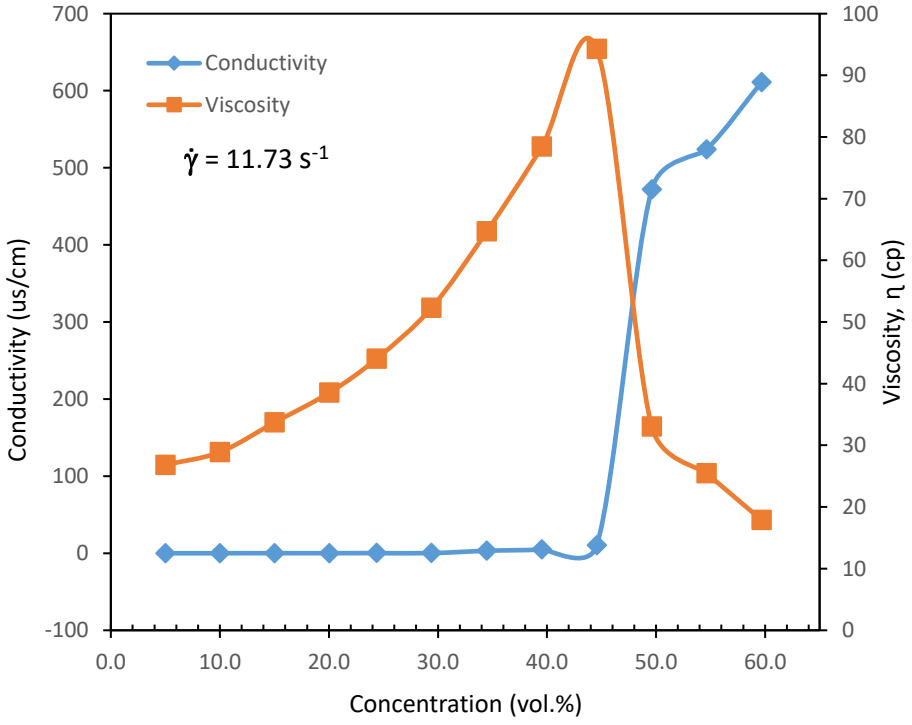
Conductivity
Viscosity
$\dot{\gamma}$ = 11.73 s^{-1}
Conductivity (us/cm)
Viscosity, η (cp)
Concentration (vol.%)
700
600
500
400
300
200
100
0
-100
100
90
80
70
60
50
40
30
20
10
0
0.0
10.0
20.0
30.0
40.0
50.0
60.0

(c)

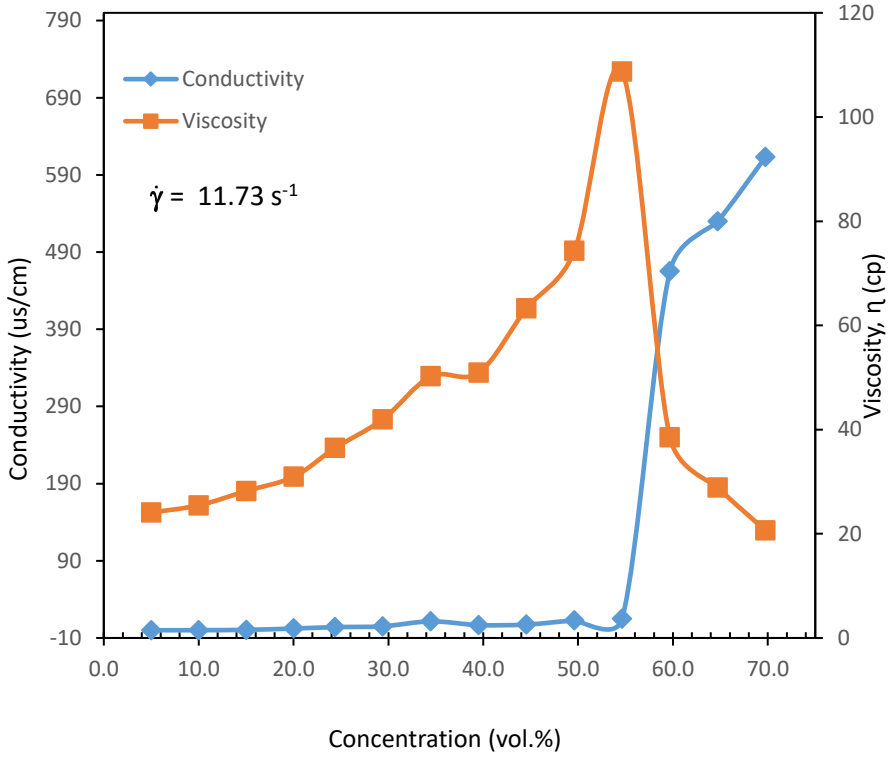

(d)

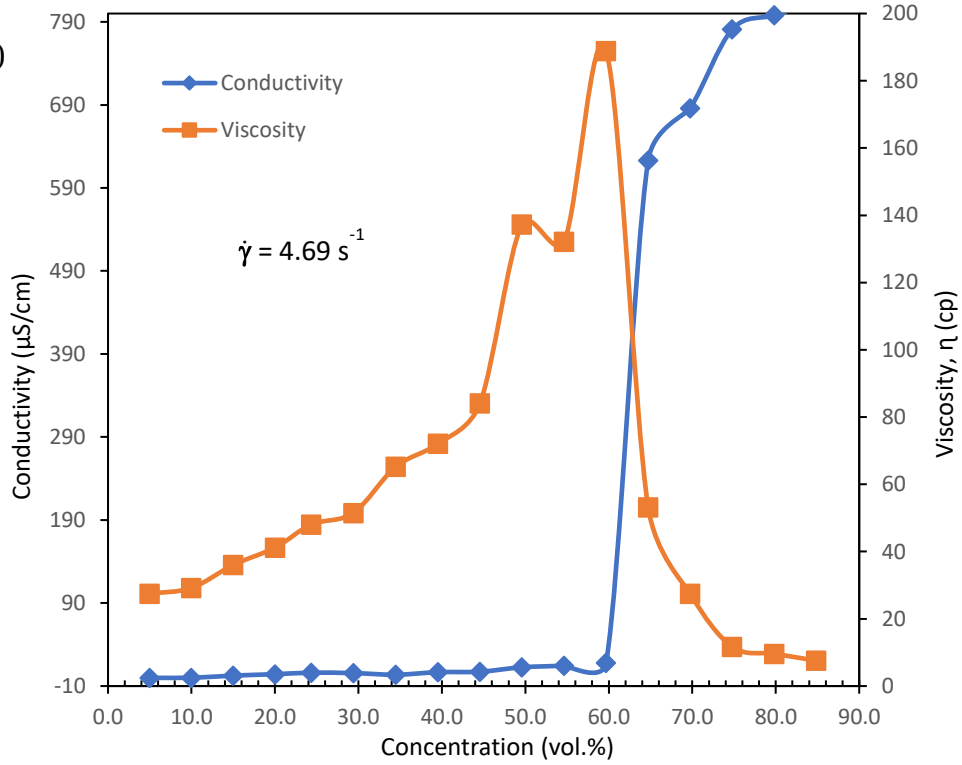

Figure 4.15 Viscosity and conductivity plots for different wt.% SNPs (a) 0.25%, (b) 0.5%, (c) 1%, (d) 2%.

4.4 Stability

To accomplish this goal, 35% W/O and 70% O/W emulsions were prepared with different concentrations of starch nanoparticles and under same processing conditions. Emulsions were quickly transferred to 100ml graduated cylinder after 15 min of mixing. Samples prepared in this manner were examined and compared both initially and over time. Stability of W/O and O/W emulsions was determined based on visual inspection. All the prepared emulsions were unstable and there was visible phase separation of the emulsions shortly after the mixing stopped. The resultant O/W emulsions and W/O emulsions are shown in Figure 4.22. Sub figure (a) shows the W/O emulsions with 35% dispersed phase by volume and (b) shows O/W emulsions with 70% dispersed phase by volume.

Following preparation, the fresh emulsions were placed in the 100ml graduated cylinder to study phase separation over the period of time. When emulsions were stored at room temperature of 21 C° for 24 hrs, they destabilized, and phase separated, leaving the clear oil and water phases behind. This may have been due to the low amount of NPs in these emulsion which was inadequate to fully stabilize high dispersed phase content present. Stability for both sets of emulsions O/W and W/O was very low as compared to emulsion made in the previous study. However, O/W emulsions lasted a couple of minutes more comparatively to W/O emulsions. It can also be seen that higher the concentrations of nanoparticle in the aqueous phase, more stable the oil-in-water emulsions and thus longer separation time. No effect of particle concentration was seen in water-in-oil emulsion type.

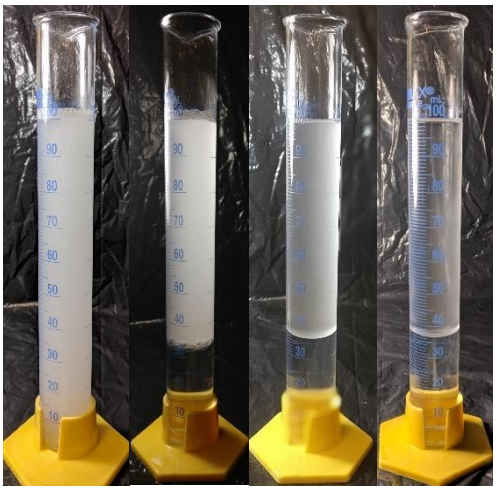

(a) Water-in-oil emulsions collected at 35% volume fraction of dispersed phase (SNPs dispersion).

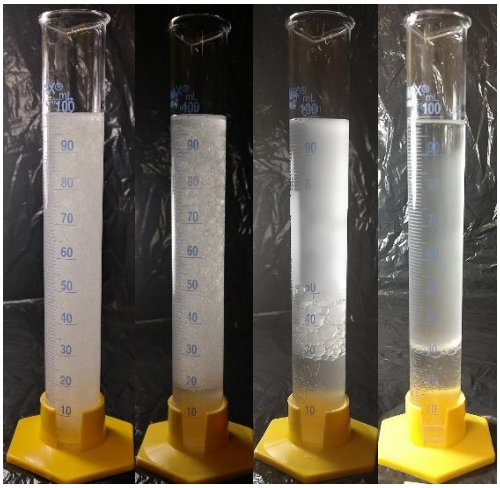

(b) Oil-in-water emulsions collected at 70% volume fraction of dispersed phase (oil).

Figure 4.16 Emulsions prepared using 0.25% wt. solid-nanoparticles. All samples were monitored for time intervals at 0, 1 min, 10 min and 24 hours mark.

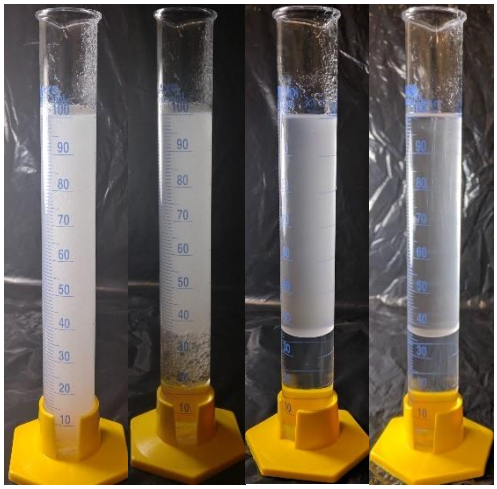

(a) Water-in-oil emulsions collected at 35% volume fraction of dispersed phase (SNPs dispersion).

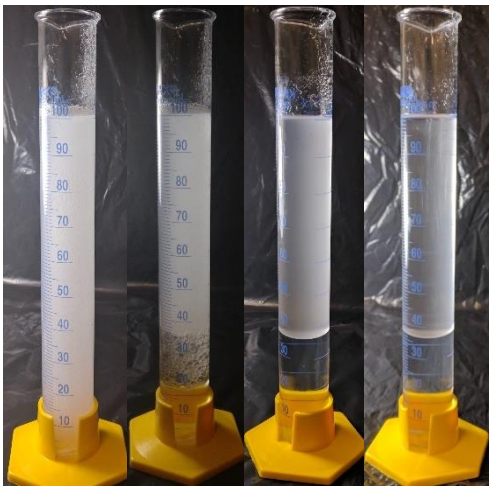

(b) Oil-in-water emulsions collected at 70% volume fraction of dispersed phase (oil).

Figure 4.17 Emulsions prepared using 0.5% wt. solid-nanoparticles. All samples were monitored for time intervals at 0, 1 min, 10 min and 24 hours mark.

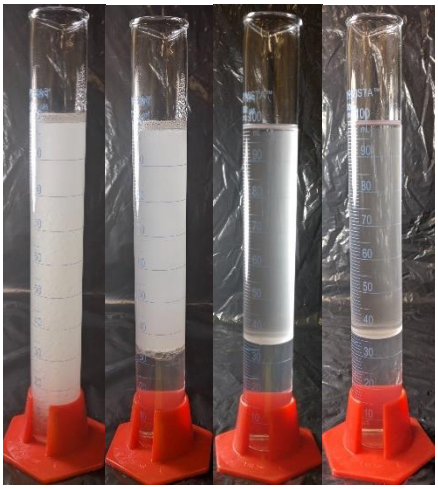

(a) Water-in-oil emulsions collected at 35% volume fraction of dispersed phase (SNPs dispersion).

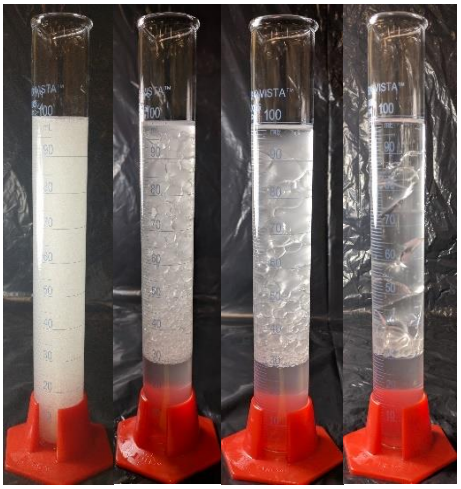

b) Oil-in-water emulsions collected at 70% volume fraction of dispersed phase (oil).

Figure 4.18 Emulsions prepared using 1% wt. solid-nanoparticles. All samples were monitored for time intervals at 0, 1 min, 10 min and 24 hours mark.

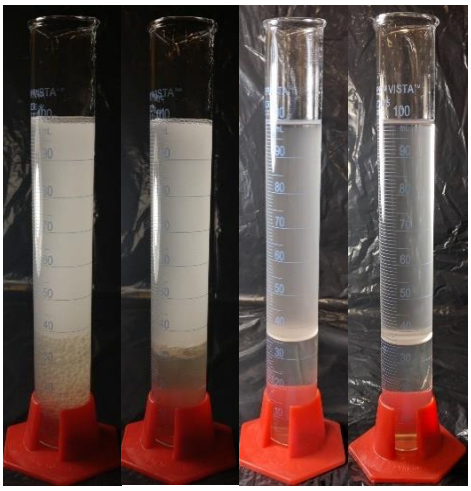

(a) Water-in-oil emulsions collected at 35% volume fraction of dispersed phase (SNPs dispersion).

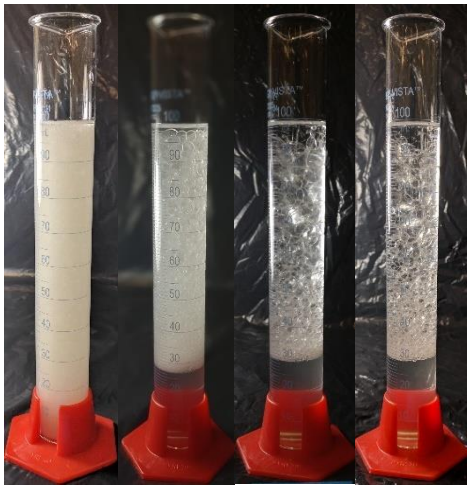

(b) Oil-in-water emulsions collected at 70% volume fraction of dispersed phase (oil).

Figure 4.19 Emulsions prepared using 2% wt. solid-nanoparticles. All samples were monitored for time intervals at 0, 1 min, 10 min and 24 hours mark.

4.5 Microscopic Observation

Images of the unstable O/W emulsions produced with 70% of the dispersed phase (oil) are shown in figure 4.18A-C. Droplets of nanoparticles emulsions were perfectly spherical with large diameter up to approximatively 500µm. The influence of nanoparticles concentrations on the resulting initial droplet diameter can be clearly seen in figure 4.18A-C.

As the particle concentration was increased the stability of NPs emulsions were enhanced. As the particle concentration is increased, the average droplet size is decreased. 2% wt. NPs oil-in-water emulsions resulted in smaller droplet size. At same concentration of NPs, water-in-oil emulsions separated extremely fast. On the other hand, the droplet sizes don't change significantly between 1% and 0.5% NPs, so the effect of nanoparticles becomes negligible at very low concentration. It is also believed that as the phase ratio is increased, it affects the viscosity and also the stability of the emulsions. All the images shown in figure 4.18 are oil droplets in water phase which can be seen thorough microscope right after preparation. Overall, increasing nanoparticle concentrations is shown to decrease droplet diameter.

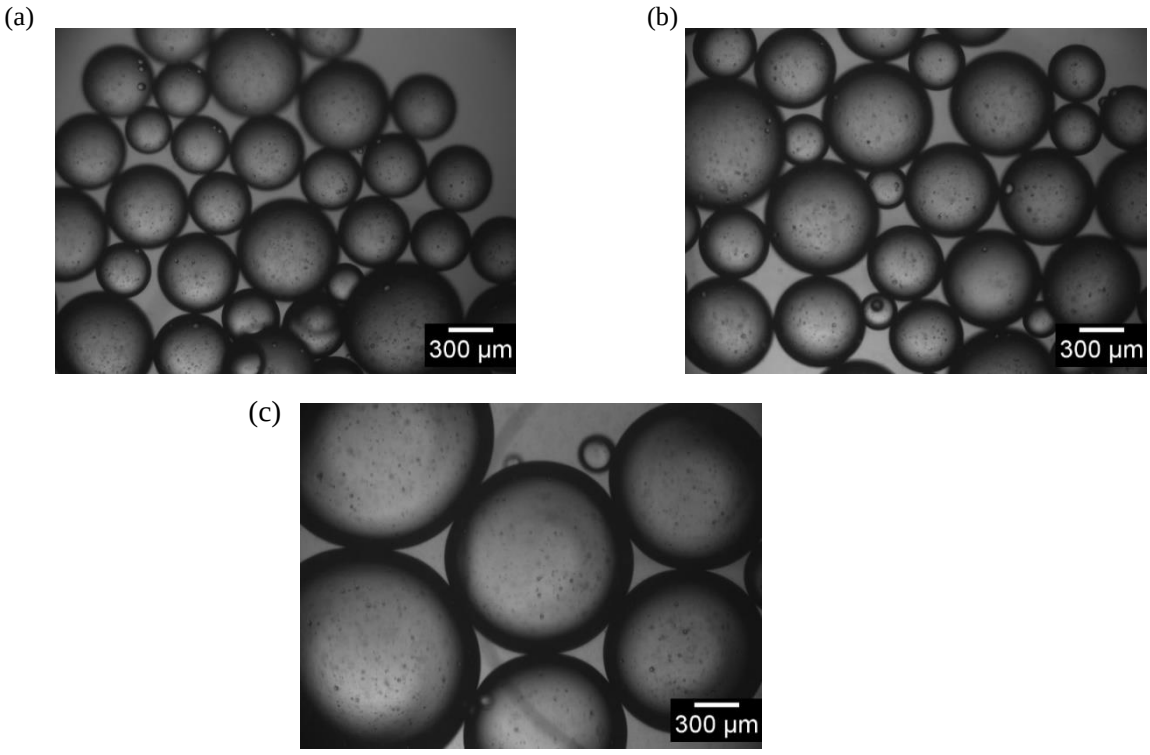

Figure 4.20 Photomicrograph of (a) 2% wt. SNPs O/W emulsions, (b) 1% wt. SNPs O/W emulsions, (c) 0.5% wt. SNPs O/W emulsions

For solid nanoparticle, interfacial wettability is an important factor in estimating the emulsion type and stability. The three-phase contact angle shows the relative position of a solid

particle at the oil-water interface. In a Pickering emulsion, contact angle shows the relative position of the particles at the water-oil interface (figure 4.19). For hydrophilic particles, the contact angle is less than 90°, and the larger surface of the solid nanoparticle would be in the water than in oil. On the same footing, contact angle for hydrophobic particles is greater than 90° and particles exist more in oil than in water.

In our work, starch nanoparticles tend to favor oil-in-water type emulsions. It is likely that due to hydrophilic nature of the nanoparticles, the contact angle formation at the oil-water interface in <90°. Consequently, phase inversion is triggered in water-in-oil type emulsions as the dispersed phase volume is increased. As we have also previously seen, the phase inversion point shifted from 44.6 vol.% to 64.7 vol.% of the dispersed phase with the increase in starch nanoparticle concentration. This trend implies that to generate a phase inversion at higher nanoparticle concentration, a more internal phase volume is required.

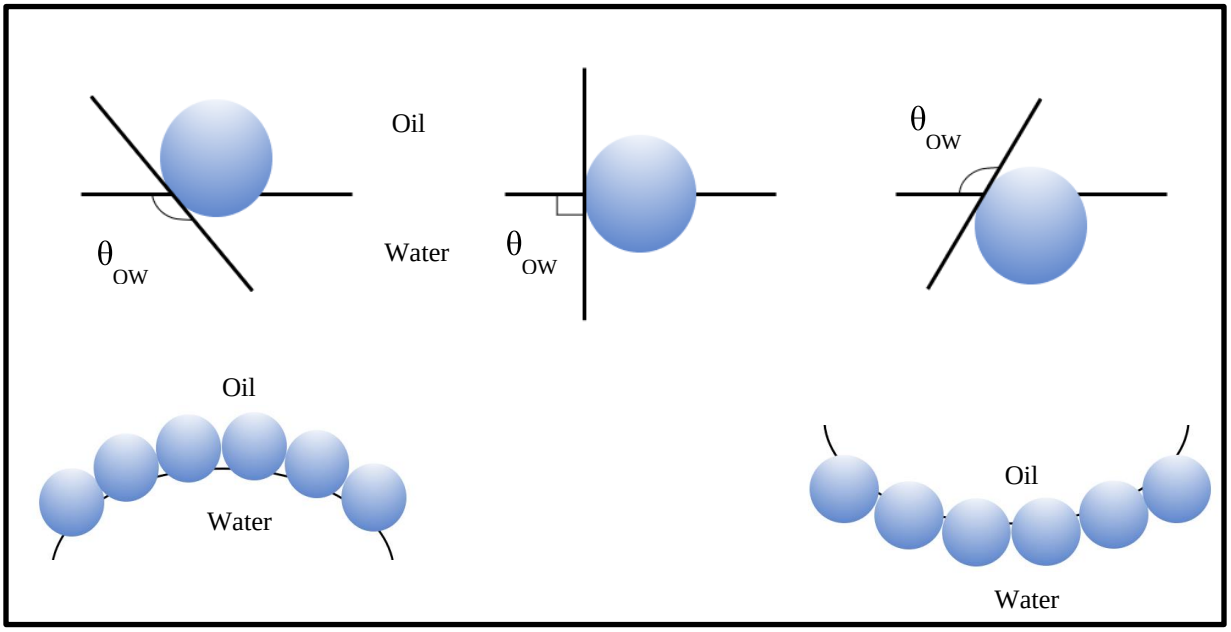

Figure 4.21 Schematic representation of solid nanoparticle forming contact angle θ at oil-water interface

As discussed earlier in the results, oil-in-water emulsions are relatively more stable than the water-in-oil emulsions. Emulsion stability depends upon the rate at which the droplets coalesces and separated from emulsions. The higher the stability of the droplets, the slower is

the rate of coalescence, and hence the delayed is phase separation. In our work, coalescence rate of the droplets decreased with the increase in starch concentration.

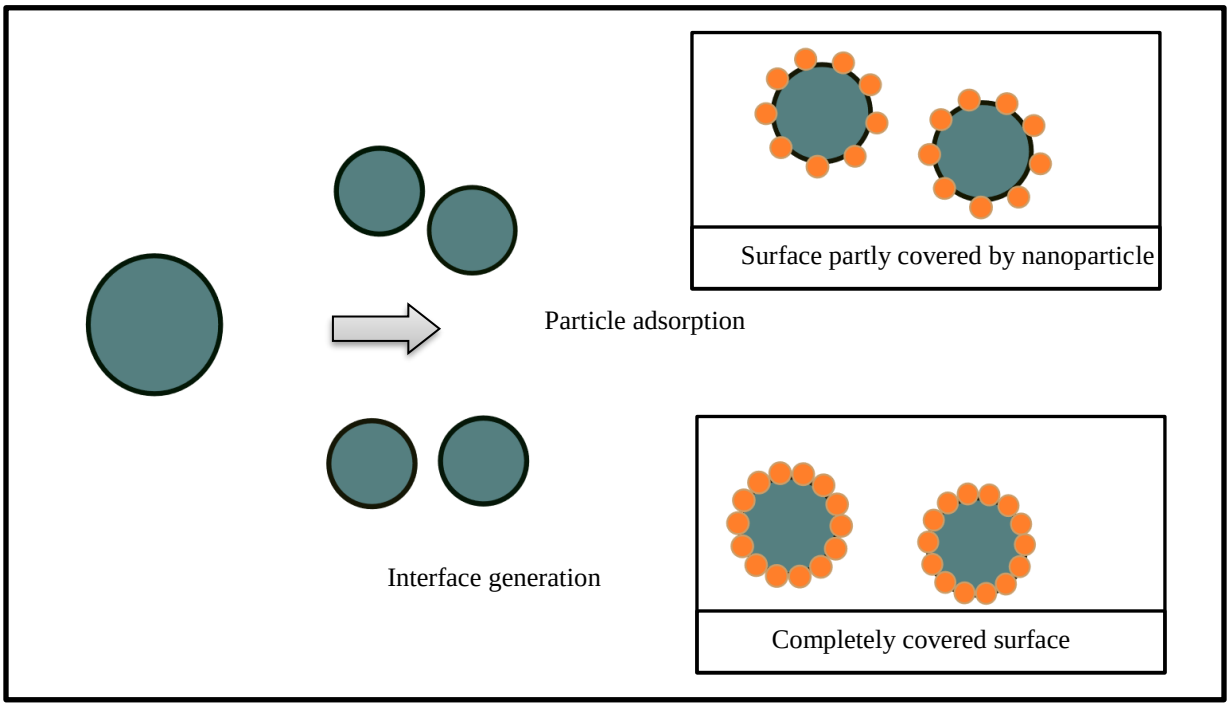

Figure 4.22 Schematic representation of particle adsorption at the droplet surface

Coalescence frequency also depends upon the particle coverage fraction as shown in figure 4.20. We assume that droplets are initially produced by mixing and shearing. In our study, mixing conditions were kept identical in all the experiments. Generation of interface leads to adsorption of particle adsorption at the interface. Droplets with the different surface area are generated depending upon the number of particles available. Coalescence is higher in droplets that are not initially covered than with saturated droplets. As we increase the concentration of the starch nanoparticles from 0.25 wt% to 2 wt%, more nanoparticles are available to completely cover the interface. Until a limiting size is reached, droplet size is controlled by the amount of SNPs concentration.

Chapter 5
Conclusions

The work is directed at delivering a viscosity measurement technique that can address the limitations of multiphase viscosity measurement by sampling. A rotational viscometer was installed in a transparent glass tank to measure the viscosity of unstable Pickering emulsions. Although, the setup did not provide extreme details about the viscosity behaviour of emulsions, but the measurements were quick and reproducible.

First of all, rheology of an oil-in-water emulsion stabilized with surfactant (Triton X-100) and starch nanoparticle was investigated. Prior to viscosity measurements of starch nanoparticle emulsion, a surfactant was employed to prepare stable O/W emulsions and understand the various factor in play while making measurements in this system. The viscosity of starch nanoparticle emulsions was significantly influenced by the dispersed phase concentration. Pickering O/W emulsions exhibited a shear thinning behavior where as the shear rate increased, the viscosity was found to decrease. Finally, the obtained experimental results were compared with emulsions prepared by surfactant and environmental friendly SNPs. The droplets of emulsions prepared with starch nanoparticle were the order of magnitude greater than the surfactant-stabilized emulsion droplet. Over the time, the surfactant emulsions showed little change except for gravitational creaming at the bottom. On the other hand, O/W emulsions with nanoparticles droplet grew bigger over time and showed noticeable phase separation.

Viscosity and conductivity were used to study the rheology of water-in-oil Pickering emulsions and to detect the phase inversion points. Catastrophic phase inversion can be triggered by the addition of the starch nanoparticle dispersion in the aqueous phase. In each case, the transition point was caught by both viscometer and conductivity readings. Nanoparticles delay the catastrophic phase inversion with an increase in particle concentrations. At 0.25 wt% of starch nanoparticles, the phase inversion occurs at 44.6 volume percent as compared to 64.7 volume percent of dispersed phase given by 2 wt% of particles. Phase inversion was delayed as the concentration of nanoparticles were increased. Also, the droplet size of the emulsion was seen to effected by the concentration of the nanoparticle.

References

[1] Schramm L L 1992 Petroleum Emulsions *Emulsions* Advances in Chemistry vol 231(American Chemical Society)pp 1–49

[2] McClements D J 1999 Context and Backgound *Food Emulsions: Principles, Practice and Tecniques* (Boca Raton, Fla. ; London: CRC Press) pp 2–5

[3] Florence A T and Rogers J A 1971 Emulsion stabilization by non-ionic surfactants: experiment and theory* *J. Pharm. Pharmacol.* **23** 233–51

[4] Yang Y, Leser M E, Sher A A and McClements D J 2013 Formation and stability of emulsions using a natural small molecule surfactant: Quillaja saponin (Q-Naturale®) *Food Hydrocoll.* **30** 589–96

[5] Chevalier Y and Bolzinger M-A 2013 Emulsions stabilized with solid nanoparticles: Pickering emulsions *Colloids Surfaces A Physicochem. Eng. Asp.* **439** 23–34

[6] Ge S, Xiong L, Li M, Liu J, Yang J, Chang R, Liang C and Sun Q 2017 Characterizations of Pickering emulsions stabilized by starch nanoparticles: Influence of starch variety and particle size *Food Chem.* **234** 339–47

[7] Dargahi-Zaboli M, Sahraei E and Pourabbas B 2017 Hydrophobic silica nanoparticle-stabilized invert emulsion as drilling fluid for deep drilling *Pet. Sci.* **14** 105–15

[8] Hohl L, Röhl S, Stehl D, von Klitzing R and Kraume M 2016 Influence of Nanoparticles and Drop Size Distributions on the Rheology of w/o Pickering Emulsions *Chemie Ing. Tech.* **88** 1815–26

[9] Leal-Calderon F, Bibette J and Schmitt V 2007 Phase Inversion *Emulsion Science: Basic Principles* (New York, NY: Springer New York) pp 11–5

[10] Perazzo A, Preziosi V and Guido S 2015 Phase inversion emulsification: Current understanding and applications *Adv. Colloid Interface Sci.* **222** 581–99

[11] Ogunlaja S B, Pal R and Sarikhani K 2018 Effects of starch nanoparticles on phase inversion

of Pickering emulsions *Can. J. Chem. Eng.* **9999** 1–9

[12] Hunter R J 2001 Thermodynamics of Surfaces *Foundations of Colloid Science* (New York, NY: Oxford University Press) pp 59–80

[13] Walstra P 1996 Emulsion Stability *Encyclopedia of Emulsion Technology* ed P Becher (New York, NY: Marcel Dekker, Inc.) pp 16–30

[14] Islam R, Rahman M, Ahmed S and Halder M R 2016 A Coaxial Cylinder Type Rotational Viscometer- Design and Optimization *Int. J. Sci. &Engineering Res.* **7** 1792–6

[15] Salas-Bringas C, Jeksrud W K and Schüller R B 2007 A new on-line process rheometer for highly viscous food and animal feed materials *J. Food Eng.* **79** 383–91

[16] Cho Y I, Kim W-T and Kensey K R 1999 A new scanning capillary tube viscometer *Rev. Sci. Instrum.* **70** 2421–3

[17] Wang G, Tan C and Li F 2017 A contact resonance viscometer based on the electromechanical impedance of a piezoelectric cantilever *Sensors Actuators A Phys.* **267** 401–8

[18] Viswanath D S, Ghosh T K, Prasad D H L, Dutt N V K and Rani K Y 2007 Rotational Viscometers *Viscosity of Liquids Theory, Estimation, Experiment, and Data* (Springer New York) pp 65–6

[19] Cheng D C H and Davis J B 1969 An automatic on-line viscometer for the measurement of non-Newtonian viscosity for process control applications *Rheol. Acta* **8** 161–73

[20] Kawatra S K and Bakshi A K 1998 On-line measurement of slurry rheology in a thickener at a copper concentrator *Miner. Metall. Process.* **15**

[21] Pipe C J, Majmudar T S and McKinley G H 2008 High shear rate viscometry *Rheol. Acta* **47** 621–42

[22] Zahirovic S, Lubansky A S, Leong Yeow Y and Boger D V. 2009 Obtaining the steady shear rheological properties and apparent wall slip velocity data of a water-in-oil emulsion from gap-dependent parallel plate viscometry data *Rheol. Acta* **48** 221–9

[23] Završnik M and Joseph-strasser M 2013 Inline viscometery for non-Newtonian viscosity characterization 587–91

[24] Steiner G, Gautsch J, Breidler R and Plank F 2010 A novel fluid dynamic inline viscometer suitable for harsh process conditions *Procedia Eng.* **5** 1470–3

[25] Kawatra S K and Bakshi A K 1995 On-Line Viscometry in Particulate Processing *Miner. Process. Extr. Metall. Rev.* **14** 249–73

[26] Kim S, Cho Y I, Kensey K R, Pellizzari R O and Stark P R H 2000 A scanning dual-capillary-tube viscometer *Rev. Sci. Instrum.* **71** 3188–92

[27] Kawatra S ., Bakshi A . and Eisele T . 1999 An on-line pressure vessel rheometer for slurries *Powder Technol.* **105** 418–23

[28] Akpek A, Youn C and Kagawa T 2014 A Study on Vibrational Viscometers Considering Temperature Distribution Effect *JFPS Int. J. Fluid Power Syst.* **7** 1–8

[29] Yabuno H, Higashino K, Kuroda M and Yamamoto Y 2014 Self-excited vibrational viscometer for high-viscosity sensing *J. Appl. Phys.* **116** 124305

[30] Higashino K, Yabuno H, Aono K, Yamamoto Y and Kuroda M 2015 Self-Excited Vibrational Cantilever-Type Viscometer Driven by Piezo-Actuator *J. Vib. Acoust.* **137** 61009

[31] Chang V, Zambrano A, Mena M and Millan A 1995 A sensor for on-line measurement of the viscosity of non-Newtonian fluids using a neural network approach *"Sensors Actuators, A Phys.* **47** 332–6

[32] Bousmina M, Ait-Kadi A and Faisant J B 1999 Determination of shear rate and viscosity from batch mixer data *J. Rheol. (N. Y. N. Y).* **43** 415–33

[33] Aït-Kadi A, Marchal P, Choplin L, Chrissemant A-S and Bousmina M 2002 Quantitative Analysis of Mixer-Type Rheometers using the Couette Analogy *Can. J. Chem. Eng.* **80** 1166–74

[34] Glenn T A and Daubert C R 2003 A mixer viscometry approach for blending devices *J. Food Process Eng.* **26** 1–16

[35] Guillemin J P, Menard Y, Brunet L, Bonnefoy O and Thomas G 2008 Development of a new mixing rheometer for studying rheological behaviour of concentrated energetic suspensions *J. Nonnewton. Fluid Mech.* **151** 136–44

Appendix A

Oil-in-water Emulsion Systems

Surfactant added oil-in-water emulsions

Conc. (%)	Temp. (C°)	Conductivity (µS/cm)	Speed (RPM)	Dial (Ø)	Shear rate (1/sec)	Shear Stress (mPa)	Viscosity (mPa.s)
1.9	24.2	1034	60	11.5	73.56	84.41	1.147
4.0	26	994	60	13	73.56	95.42	1.297
6.0	27.3	966	60	12.5	73.56	91.75	1.247
			30	7	36.78	51.38	1.397
8.0	21.6	951	60	14.5	73.56	106.43	1.447
			30	7.5	36.78	55.05	1.497
10.0	24.7	915	60	14.5	73.56	106.43	1.447
			30	8	36.78	58.72	1.597
15.0	26	835	60	16.5	73.56	121.11	1.646
			30	8.5	36.78	62.39	1.696
20.0	26	792	60	19	73.56	139.46	1.896
			30	10.5	36.78	77.07	2.095
25.0	22.6	702	60	26	73.56	190.84	2.594
			30	14	36.78	102.76	2.794
30.0	26.1	586	60	32.5	73.56	238.55	3.243
			30	18.5	36.78	135.79	3.692
35.0	28.5	510	60	41	73.56	300.94	4.091
			30	21.5	36.78	157.81	4.291
			12	10.5	14.71	77.07	5.239

39.9	28.6	488	60	59.5	73.56	436.73	5.937
			30	29	36.78	212.86	5.787
			12	14	14.712	102.76	6.985
44.9	26	430	60	81.5	73.56	598.21	8.132
			30	46	36.78	337.64	9.18
			12	22	14.71	161.48	10.98
49.9	25.5	396	30	60	36.78	440.4	11.97
			12	28	14.712	205.52	13.97
			6	15.5	7.356	113.77	15.47
54.8	25.3	341	12	37.5	14.71	275.25	18.709
			6	22	7.356	161.48	21.952
			3	12.5	3.678	91.75	24.95
59.9	26	286	6	40	7.356	293.6	39.91
			3	22	3.678	161.48	43.90
			1.5	13.5	1.839	99.09	53.88

Starch Nanoparticle oil-in-water emulsions

Conc. (%)	Conductivity (µS/cm)	Temp. (C°)	Speed (RPM)	Dial (Ø)	Shear rate (1/sec)	Shear Stress (mPa)	Viscosity (mPa.s)
1.9	961	26.7	60	16.5	73.56	121.11	1.65
			30	8.5	36.78	62.39	1.70
4.0	933	27.5	60	17.5	73.56	128.45	1.75
			30	9	36.78	66.06	1.80
6.0	908	27.5	60	16.5	73.56	121.11	1.65
			30	8.5	36.78	62.39	1.70
8.0	877	28.1	60	17.5	73.56	128.45	1.75
			30	9.5	36.78	69.73	1.90
10.0	854	28.1	60	17	73.56	124.78	1.70
			30	11	36.78	80.74	2.20
12.0	814	28.9	60	20.5	73.56	150.47	2.05
			30	9.5	36.78	69.73	1.90
14.0	793	27.9	60	23.5	73.56	172.49	2.34
			30	10	36.78	73.4	2.00
16.0	764	27.9	60	28	73.56	205.52	2.79
			30	12.5	36.78	91.75	2.49
18.0	737	28.2	60	30	73.56	220.2	2.99
			30	19.5	36.78	143.13	3.89
20.1	707	28.3	60	40.5	73.56	297.27	4.04
			30	20	36.78	146.8	3.99
25.1	637	28.5	60	48.5	73.56	355.99	4.84
			30	30.5	36.78	223.87	6.09

30.0	572	29.1	60	61	73.56	447.74	6.09
			30	40	36.78	293.6	7.98
			12	23.5	14.712	172.49	11.72
35.1	520	29	60	86.5	73.56	634.91	8.63
			30	57.5	36.78	422.05	11.47
			12	34	14.712	249.56	16.96
			6	25	7.356	183.5	24.95
40.0	466	29.4	30	80	36.78	587.2	15.97
			12	44.5	14.712	326.63	22.20
			6	21	7.356	154.14	20.95
			60	33.5	23.46	540.02	23.02
			30	25.5	11.73	411.06	35.04
45.0	419	28.6	30	75	36.78	550.5	14.97
			12	53	14.712	389.02	26.44
			6	34.5	7.356	253.23	34.42
			60	42	23.46	677.04	28.86
			30	29.5	11.73	475.54	40.54
50.0	371	28.9	12	57	14.712	418.38	28.44
			6	43	7.356	315.62	42.91
			3	24	3.678	176.16	47.90
			60	51.5	23.46	830.18	35.39
			30	38	11.73	612.56	52.22
54.9	319	29.4	6	60	7.356	440.4	59.87
			3	56	3.678	411.04	111.76
			1.5	37	1.839	271.58	147.68

			0.6	29	0.7356	212.86	289.37
			0.3	27	0.3678	198.18	538.83
			60	68	23.46	1096.16	46.72
			30	50	11.73	806	68.71
			12	30	4.692	483.6	103.07
59.9	277.3	29.5	3	60	3.678	440.4	119.74
			1.5	52	1.839	381.68	207.55
			0.6	32	0.7356	234.88	319.30
			30	69	11.73	1112.28	94.82
			12	48	4.692	773.76	164.91
			6	37	2.346	596.44	254.24
			3	30.5	1.173	491.66	419.15
64.9	221	28	12	75	4.692	1209	257.67
			6	58	2.346	934.96	398.53
			3	49.5	1.173	797.94	680.26
			1.5	38.5	0.5865	620.62	1058.18
			0.3	20	0.1173	322.4	2748.51
69.9	183.4	28.1	3	80	1.173	1289.6	1099.40
			1.5	57	0.5865	918.84	1566.65
			0.6	32.5	0.2346	523.9	2233.16
74.9	140.5	28.6	3	72	1.173	1160.64	989.46
			1.5	53	0.5865	854.36	1456.71
			0.6	31.5	0.2346	507.78	2164.45
79.9	88	28.3	12	54	4.692	870.48	185.52
			6	31	2.346	499.72	213.01

			3	19.5	1.173	314.34	267.98

Surfactant oil-in-water emulsions from Offline Viscometer

Conc. (%)	Speed (RPM)	Dial (Ø)	Shear rate (1/sec)	Shear Stress (mPa)	Viscosity (mPa.s)
1.94	600	12	1020.8	999.6	0.98
	300	7	510.9	523.6	1.02
3.95	600	13	1020.8	1094.8	1.07
	300	7	510.9	523.6	1.02
5.96	600	12	1020.8	999.6	0.98
	300	7	510.9	523.6	1.02
7.97	600	14	1020.8	1190	1.17
	300	8	510.9	618.8	1.21
9.97	600	14	1020.8	1190	1.17
	300	8	510.9	618.8	1.21
15	600	17	1020.8	1475.6	1.45
	300	9	510.9	714	1.40
20.01	600	24	1020.8	2142	2.10
	300	13	510.9	1094.8	2.14
29.96	600	35	1020.8	3189.2	3.12
	300	18	510.9	1570.8	3.07

34.98	600	46	1020.8	4236.4	4.15
	300	23	510.9	2046.8	4.01
39.9	600	52	1020.8	4807.6	4.71
	300	28	510.9	2522.8	4.94
	200	19	340.6	1666	4.89
44.91	600	75	1020.8	6997.2	6.85
	300	39	510.9	3570	6.99
	200	27	340.6	2427.6	7.13
	180	24	306.02	2142	7.00
49.92	600	117	1020.8	10995.6	10.77
	300	55	510.9	5093.2	9.97
	180	35	306.02	3189.2	10.42
54.84	600	159	1020.8	14994	14.69
	300	85	510.9	7949.2	15.56
	200	60	340.6	5569.2	16.35
	100	32	170.3	2903.6	17.05
59.86	600	214	1020.8	20230	19.82
	300	121	510.9	11376.4	22.27
	200	86	340.6	8044.4	23.62
	100	48	170.3	4426.8	25.99

Appendix B

Water-in-Oil Emulsion Systems

0.25% wt. starch nanoparticles

Conc. (%)	Conductivity (µS/cm)	Temp. (C°)	Speed (RPM)	Dial (Ø)	Shear rate (1/sec)	Shear Stress (mPa)	Viscosity (mPa.s)
5.01	0	23.1	60	50	23.46	807	**34.40**
			30	25	11.73	403.5	**34.40**
			12	8.5	4.692	137.19	**29.24**
10.0	0	23.6	60	53	23.46	855.42	**36.46**
			30	27	11.73	435.78	**37.15**
			12	11.5	4.692	185.61	**39.56**
15.0	0	25.4	60	59	23.46	952.26	**40.59**
			30	30	11.73	484.2	**41.28**
			12	11	4.692	177.54	**37.84**
20.0	0	25.8	60	65.5	23.46	1057.17	**45.06**
			30	34	11.73	548.76	**46.78**
			12	13	4.692	209.82	**44.72**
24.4	0.03	26.2	60	78	23.46	1258.92	**53.66**
			30	38.5	11.73	621.39	**52.97**
			12	15.5	4.692	250.17	**53.32**
29.4	0.15	25.8	60	89.5	23.46	1444.53	**61.57**
			30	47	11.73	758.58	**64.67**
			12	17.5	4.692	282.45	**60.20**
34.5	0.22	26.6	30	57	11.73	919.98	**78.43**
			12	20	4.692	322.8	**68.80**
			6	9	2.346	145.26	**61.92**
39.5	0.34	26.6	30	68.5	11.73	1105.59	**94.25**
			12	24	4.692	387.36	**82.56**
			6	12	2.346	193.68	**82.56**
44.6	334	26.5	60	41	23.46	661.74	**28.21**
			30	28	11.73	451.92	**38.53**
			12	13	4.692	209.82	**44.72**
49.6	418	26.3	60	27.5	23.46	443.85	**18.92**
			30	16.5	11.73	266.31	**22.70**
			12	12	4.692	193.68	**41.28**
54.6	475	26.5	60	20	23.46	322.8	**13.76**

			30	13	11.73	209.82	17.89
11.1	543	26.1	60	15	23.46	242.1	10.32
			30	12	11.73	193.68	16.51

0.5% wt. starch nanoparticles

Conc. (%)	Conductivity (µS/cm)	Temp. (C°)	Speed (RPM)	Dial (Ø)	Shear rate (1/sec)	Shear Stress (mPa)	Viscosity (mPa.s)
5.01	0	22	60	40	23.46	645.6	27.52
			30	19.5	11.73	314.73	26.83
			12	7	4.692	112.98	24.08
10.0	0	23.1	60	43	23.46	694.02	29.58
			30	21	11.73	338.94	28.90
			12	9	4.692	145.26	30.96
15.0	0.05	24	60	49.5	23.46	798.93	34.05
			30	24.5	11.73	395.43	33.71
			12	10	4.692	161.4	34.40
20.0	0.07	25	60	54	23.46	871.56	37.15
			30	28	11.73	451.92	38.53
			12	11	4.692	177.54	37.84
24.4	0.11	25.6	60	63.5	23.46	1024.89	43.69
			30	32	11.73	516.48	44.03
			12	14	4.692	225.96	48.16

29.4	0.17	25.9	60	77	23.46	1242.78	52.97
			30	38	11.73	613.32	52.29
			12	14.5	4.692	234.03	49.88
34.5	3.17	26.2	60	90	23.46	1452.6	61.92
			30	47	11.73	758.58	64.67
			12	18	4.692	290.52	61.92
39.5	4.84	26.1	30	57	11.73	919.98	78.43
			12	22	4.692	355.08	75.68
			6	10	2.346	161.4	68.80
44.6	10.21	26.3	30	68.5	11.73	1105.59	94.25
			12	26.5	4.692	427.71	91.16
			6	13	2.346	209.82	89.44
49.6	472	27.5	60	35	23.46	564.9	24.08
			30	24	11.73	387.36	33.02
			12	12	4.692	193.68	41.28
54.6	524	28	60	27.5	23.46	443.85	18.92
			30	18.5	11.73	298.59	25.46
			12	10	4.692	161.4	34.40
11.1	611	27	60	20	23.46	322.8	13.76
			30	13	11.73	209.82	17.89

1% wt. starch nanoparticles

Conc. (%)	Conductivity (µS/cm)	Temp. (C°)	Speed (RPM)	Dial (∅)	Shear rate (1/sec)	Shear Stress (mPa)	Viscosity (mPa.s)
5.01	0	22	60	36	23.46	581.04	24.77
			30	17.5	11.73	282.45	24.08
			12	7	4.692	112.98	24.08
10.0	0.08	23.1	60	37	23.46	597.18	25.46
			30	18.5	11.73	298.59	25.46
			12	7.5	4.692	121.05	25.80
15.0	0.52	24	60	39	23.46	629.46	26.83
			30	20.5	11.73	330.87	28.21
			12	8	4.692	129.12	27.52
20.0	2.21	25	60	47.5	23.46	766.65	32.68
			30	22.5	11.73	363.15	30.96
			12	9	4.692	145.26	30.96
25.0	4.06	25.6	60	51.5	23.46	831.21	35.43
			30	26.5	11.73	427.71	36.46
			12	10.5	4.692	169.47	36.12
30.0	5.08	25.9	60	60.5	23.46	976.47	41.62
			30	30.5	11.73	492.27	41.97
			12	12	4.692	193.68	41.28
35.0	11.5	26.2	60	71.5	23.46	1154.01	49.19
			30	36.5	11.73	589.11	50.22
			12	15	4.692	242.1	51.60

40.0	6.71	26.1	60	83	23.46	1339.62	57.10
			30	37	11.73	597.18	50.91
			12	15.5	4.692	250.17	53.32
45.0	7.37	26.3	60	82	23.46	1323.48	56.41
			30	46	11.73	742.44	63.29
			12	17	4.692	274.38	58.48
50.0	12.63	27.5	30	54	11.73	871.56	74.30
			12	21	4.692	338.94	72.24
			6	11	2.346	177.54	75.68
55.0	14.63	28	30	79	11.73	1275.06	108.70
			12	30	4.692	484.2	103.20
			6	13	2.346	209.82	89.44
60.0	465	27	60	36	23.46	581.04	24.77
			30	28	11.73	451.92	38.53
			12	14.5	4.692	234.03	49.88
65.0	530	27	60	32	23.46	516.48	22.02
			30	21	11.73	338.94	28.90
			12	9	4.692	145.26	30.96
70.0	613	26.5	60	23	23.46	371.22	15.82
			30	15	11.73	242.1	20.64

2% wt. starch nanoparticles

Conc. (%)	Conductivity (µS/cm)	Temp. (C°)	Speed (RPM)	Dial (Ø)	Shear rate (1/sec)	Shear Stress (mPa)	Viscosity (mPa.s)
5.01	0	22	60	41	23.46	661.74	28.21
			30	20	11.73	322.8	27.52
			12	8	4.692	129.12	27.52
10.0	0.08	23.1	60	46	23.46	742.44	31.65
			30	23.5	11.73	379.29	32.34
			12	8.5	4.692	137.19	29.24
15.0	2.68	24	60	52.5	23.46	847.35	36.12
			30	27.5	11.73	443.85	37.84
			12	10.5	4.692	169.47	36.12
20.0	4.31	25	60	61	23.46	984.54	41.97
			30	30.5	11.73	492.27	41.97
			12	12	4.692	193.68	41.28
25.0	6.16	25.6	60	72.5	23.46	1170.15	49.88
			30	38.5	11.73	621.39	52.97
			12	14	4.692	225.96	48.16
30.0	5.61	25.9	60	81	23.46	1307.34	55.73
			30	44	11.73	710.16	60.54
			12	15	4.692	242.1	51.60
35.0	3.74	26.2	60	92	23.46	1484.88	63.29
			30	52.5	11.73	847.35	72.24
			12	19	4.692	306.66	65.36
40.0	6.71	26.1	30	63	11.73	1016.82	86.69
			12	21	4.692	338.94	72.24
			6	10	2.346	161.4	68.80
45.0	7.37	26.3	30	74	11.73	1194.36	101.82
			12	24.5	4.692	395.43	84.28
			6	12.5	2.346	201.75	86.00
50.0	12.63	27.5	30	90	11.73	1452.6	123.84
			12	40	4.692	645.6	137.60
			6	20	2.346	322.8	137.60
			3	9	1.173	145.26	123.84
55.0	14.63	28	12	38.5	4.692	621.39	132.44
			6	17	2.346	274.38	116.96
			3	8.5	1.173	137.19	116.96
60.0	18.02	27	12	55	4.692	887.7	189.19
			6	22.5	2.346	363.15	154.80
			3	10.5	1.173	169.47	144.48

65.0	623	27	60	39	23.46	629.46	26.83
			30	27	11.73	435.78	37.15
			12	15.5	4.692	250.17	53.32
70.0	686	26.5	60	25	23.46	403.5	17.20
			30	18	11.73	290.52	24.77
			12	8	4.692	129.12	27.52
75.0	781	25.4	60	17	23.46	274.38	11.70
			30	6	11.73	96.84	8.26
80.0	798	26.1	60	14	23.46	225.96	9.63
85.0	815	24.3	60	11	23.46	177.54	7.57